Reduced Cementitious Material in Optimized Concrete Mixtures: Annual Cell Performance Report

Contract Number: (C) 1003320 (WO) 3

Task 2B: Annual Cell Performance Report

Principal Investigator
Peter Taylor
Director
National Concrete Pavement Technology Center, Iowa State University

Co-Principal Investigator
Seyedhamed Sadati
Assistant Scientist IV
National Concrete Pavement Technology Center, Iowa State University

Performing Organization
National Concrete Pavement Technology Center
Iowa State University
2711 South Loop Drive, Suite 4700
Ames, IA 50010-8664
Phone: 515-294-8103 / Fax: 515-294-0467
www.cptechcenter.org

Sponsored by
Federal Highway Administration
Minnesota Department of Transportation
National Road Research Alliance Transportation Pooled Fund

Lead State Representative
Bernard Izevbekhai
Minnesota Department of Transportation
Office of Materials and Road Research, Mail Stop 645
1400 Gervais Avenue, Maplewood, Minnesota 55109
Phone: 651-366-5454
E-Mail: bernard.izevbekhai@state.mn.us

Table of Contents

LIST OF FIGURES

LIST OF TABLES

ACKNOWLEDGMENTS

The research team would like to express their gratitude to the Minnesota Department of Transportation (MnDOT) for sponsoring this research and the National Road Research Alliance (NRRA) for supporting this work.

INTRODUCTION

This document reports the activities and observations of a research team that performed on-site and laboratory testing of modified concrete mixtures with optimized cementitious materials content placed on two designated field testing cells at the MnROAD facility, Monticello, Minnesota.

The work explores the performance of pavement sections cast with optimized concrete mixtures proportioned with reduced binder content. Concrete paving mixtures with “low” cementitious content, i.e., 500 lb/yd^3, and “lower” cementitious content, i.e., 470 lb/yd^3, used at two identical (except for concrete mix) cells 138 and 238, respectively. Each cell is about 260 feet long. The primary goal of this work is to monitor the constructability and longevity of the concrete mixtures with reduced cementitious material content. The overall objectives of this research project include:

- Investigate the early-age characteristics (i.e. placement issues, slow strength gain) of concrete paving mixes containing reduced cementitious content
- Assess causes of, or potential for, durability issues with very low cementitious content
- Identify effect of reduced cementitious content on long term serviceability and economics of concrete pavements (i.e. benefits of reduced shrinkage)
- Develop recommended specifications, mixing and placement practices for the use of very low cementitious content concrete paving mixes

This interim report discusses data collected and observations made through the second year of exposure of the test sections.

PROJECT INFORMATION

The present project investigates the performance of two test cells (138 and 238) constructed with optimized concrete mixtures at MnROAD pavement research facility. Located in Albertville, 40 miles Northwest of Saint Paul Minnesota, the MnROAD research facility consists of two distinct segments of roadway: the Mainline (ML) and the Low Volume Road (LVR). MnROAD was built in 1993, comprising 23 original test cells at the time. As at 2016, there were a total of 69 test cells between the Mainline and LVR. A different pavement type and/or design is used in construction of each of these cells.

The Mainline is a 3.5 mile, 2-lane interstate highway that carries live traffic diverted from Westbound Interstate 94 while the LVR is a 2-lane wide closed loop with 24 test cells (in 2016) with a total length of 2.5 miles. The traffic on the LVR is restricted to a single 18-wheel, 5-axle tractor with trailer that is intended to simulate the traffic conditions on rural roads. Operation of this vehicle is performed by the MnROAD staff and according to a controlled schedule that includes 80 laps per day on the inside lane only. The outside lane is subject to environmental loading only, except for the minimal loading from lightweight test vehicles. This restriction is intended to demonstrate the pavement response due to environmental effects versus loading effects.

The low cementitious test cells 138 and 238 are contiguously located on the LVR as presented in Figure 1. A concrete mixture with 500 lb/yd^3 of cementitious materials was used for building Cell 138 and designated as the low cementitious mixture, while another similar mixture proportioned with 470 lb/yd^3 of cementitious materials content was used for Cell 238 and designated as the lower cementitious mixture in this report. Data obtained from these two cells were compared to those gathered from testing the Cell 524 proportioned with 570 lb/yd^3 of cementitious materials that serves as the reference cell in this study.

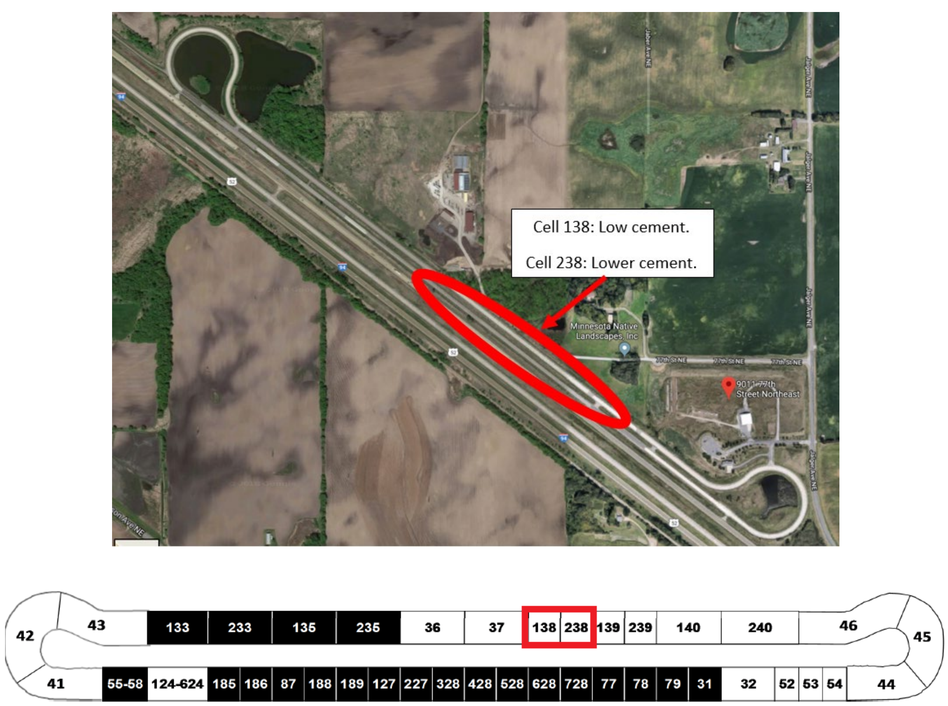

Figure 1- Aerial photo (top) and schematic view (bot.) of the investigated cells

Concrete placement, sampling, and testing for fresh properties took place on July 14, 2017. The construction activities, design details, and research activities of each test cell were identical:

- Construction activities
    - Remove 258 feet of existing concrete pavement
    - Repair existing Class 5 base (if damaged)
    - Install sensors, including vibrating wire strain gauges, quarter-bridge strain gauges, thermocouple trees and maturity loggers
    - Install T2 plates (for thickness verification)
    - Place new concrete layer and conduct tests during paving
    - Fabricate research samples (cylinders/beams) for further lab testing
    - Place new gravel shoulders
- Design details (shown in Figure 2)
    - Panel thickness = 8 inches
    - Panel size = 12 ft W x 15 ft L driving lane
    - Low cementitious mixture with 500 lb/yd^3 of cementitious materials at Cell 138 and lower cementitious mixture with 470 lb/yd^3 of cementitious materials at Cell 238
    - Shoulders = 2 inch thick shoulder gravel
    - Dowel bars = 1.25 inch diameter epoxy coated steel in standard MnDOT pattern
    - Joints = Single 0.125 inch width saw cut, depth = T/4, unsealed
    - Base: 5.0 in. Class 5 aggregate base
    - Subgrade: Clay loam (A-6)

Details regarding the concrete mixture designs, properties of the ingredients (cementitious materials and aggregates), fresh concrete properties, and hardened concrete properties were previously discussed in the first year performance report. The present report offers a summary of in-situ test results, as well as the data obtained from embedded sensors during the first two years of service. Moreover, results of a distress survey and in-situ inspection of the pavement condition are included.

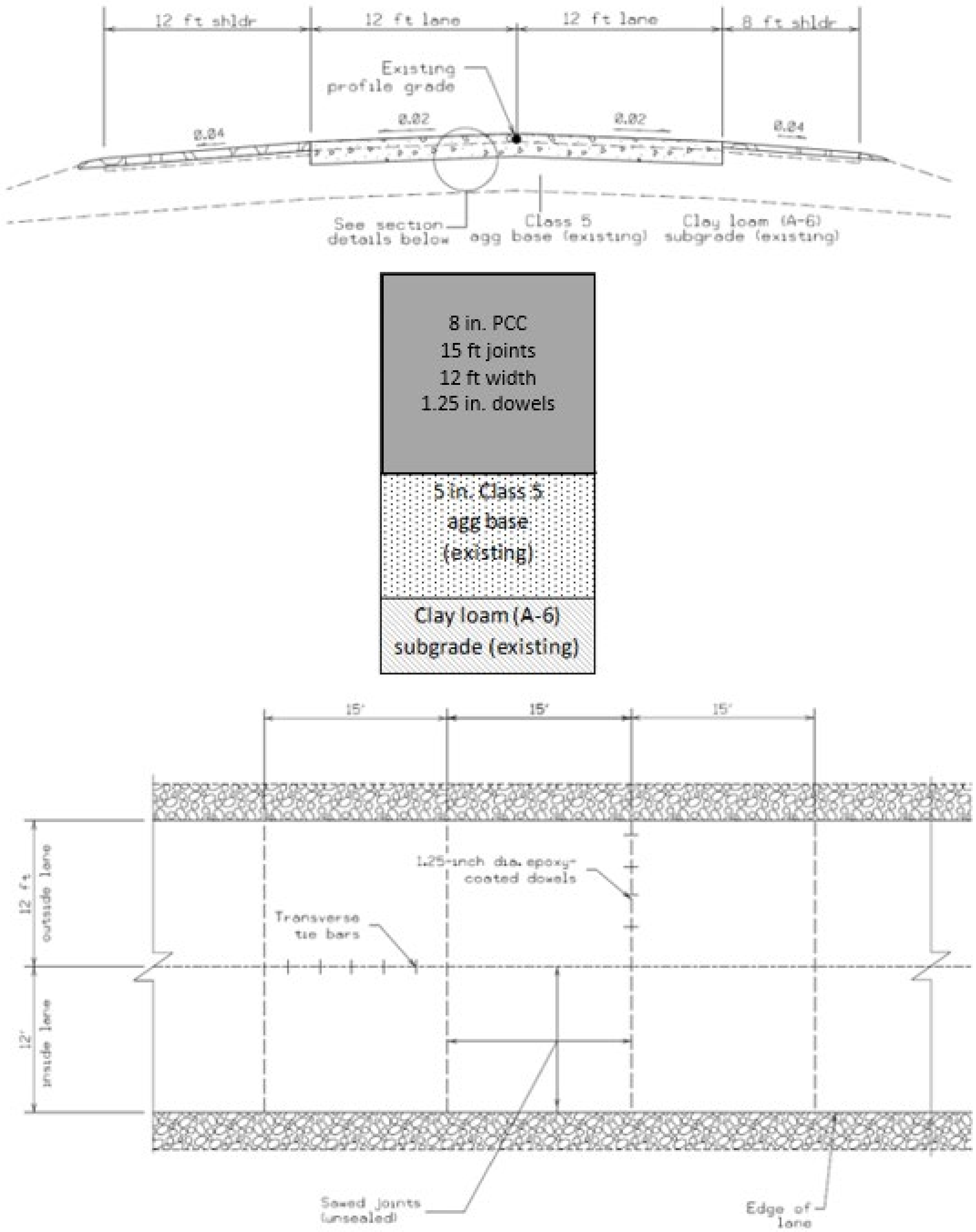

Figure 2- Pavement construction details

TEST METHODS

The work conducted investigating the properties of the test cells in their second year can be divided into two main categories:

- Use of instrumentation and in-situ tests aimed at monitoring the performance of the pavements over time.
- Field inspection to explore signs of premature distress and assessment of the pavement condition

The following instrumentations and in-situ tests were conducted based instrumentation placed and monitored by MnRROAD staff:

- Falling weight deflectometer (MnDOT's FWD Tester, ASTM E2583 07-2015)
- Ride quality (MnDOT's Light Weight Profiler, ASTM E-950)
- Dynamic load test (MnROAD Semi Tractor Trailer)
- Deformations due to environmental conditions (Vibrating Wire Strain Gages)
- Temperature gradient through the depth of pavement structure (Thermocouples)
- Moisture gradient through the depth of pavement structure (Decagon conductivity sensors)

The distress survey included the following conducted by the research team:

- In-situ inspection for evaluating signs of premature distress
- Inspection of surface texture abnormalities associated with concrete workability
- Investigating cracking occurred in test sections
- Extracting and analyzing core specimens in distressed areas

RESULTS

This section summarizes the data obtained during the first two years from construction of the investigated cells. Specific tests are discussed below.

Pavement Performance – In-Situ Measurements

Falling Weight Deflectometer

Falling weight deflectometer (FWD) test was conducted on pavement cast with reduced cement content and reference mixture according to the following matrix. Note that the reference cell (Cell 524) is 6.0 in. thick, while the 138 and 238 Cells were 8.0 in. thick. MnDOT's FWD tester, conforming to requirements of the ASTM E2583 was used for testing the cells. The test setup is shown in Figure 3 .

Figure 3- MnDOT's FWD tester

Test dates:

Reference pavement (Cell 524): 09/14/2017, 10/23/2017, 03/15/2018, and 05/04/2018. Measurements conducted in May 2018 for Cell 524 were the only additions to this section compared to the first year's performance report.

Pavement with low (Cell 138) and lower cementitious materials (Cell 238): 09/06/2017, 10/24/2017, 03/27/2018, and 05/03/2018

Investigated lanes:

Inside lane and outside lane for all cells

Investigated slabs:

Reference pavement (Cell 524): slab #0 and #2

Low cement pavement (Cell 138): slab #4, #7, #11, and #14

Lower cement pavement (Cell 238): slab #2, #6, #9, and #13

Test positions:

Slab center, corner, mid-edge, joint before, and joint after for all concrete types

Load amounts:

Deflections were collected for one drop at each load level of 6000, 9000, and 12000 lbs, corresponding to approximate stress level of 390, 570, and 750 KPa.

Sensor offsets:

Ten sensors were incorporated to collect the deformation at various distances with respect to the center of the load plate. Table 1 summarizes the sensor spacing.

Table 1- FWD sensor spacing from center of the load plate

Sensor #	1	2	3	4	5	6	7	8	9	10
Distance (in.)	0	8	12	18	24	36	48	60	72	-12

Test data obtained from FWD testing conducted before and after the transverse joints, corresponding to approaching and departure traffics, respectively, were used to calculate the load transfer efficiency (LTE) according to Equation 1.

$$LTE = \frac{\delta_U}{\delta_L} \times 100\% \tag{1}$$

where δ_U is the deflection of the unloaded side of the joint (mm), δ_L is the deflection of the loaded side of the joint (mm), and LTE is the load transfer efficiency (%).

Results are summarized in Tables 9 to 11 for the pavement cast with low cement, lower cement, and reference concrete mixtures, respectively. The values reported in these tables summarize the data obtained for both inside and outside lanes exposed to approaching and departure traffic, also known as "Before Joint" and "After Joint" measurements, respectively.

Results obtained for inside lane of Cell 138 cast with low cementitious materials content indicated LTE values ranging from 79% to 96%, and from 80% to 95% for the approach and departure traffics, respectively. LTE values obtained for the outside lane ranged from 82% to 93% and from 83% to 97% for the approach and departure traffics, respectively.

Similar data were obtained from Cell 238, indicating comparable LTE for the departure and approaching traffics for both lanes. For the inside lane, the LTE ranged from 78% to 95% for the approaching and from 82% to 97% for the departure traffic, respectively. LTE results were between 84% and 94% for the outside lanes, regardless of the traffic direction.

Slight reduction in LTE was observed for the reference pavement with average data between 85% and 91%. This can be due to the lower thickness of the reference cell compared to the low cement sections.

The LTE data are summarized in Figure 4. In general a linear correlation was observed for the LTE values obtained for the approaching and the departure traffic. In general the LTE values obtained for Cells 138 and 238 were comparable, indicating similar load transfer characteristics for these two cells. For both cells, the comparison between the LTE values for departure and approaching traffic indicated higher scatter in LTE values for the inside lane exposed to regular traffic loading. In summary, the LTE values obtained for Cells 138 and 238 suggested similar performance during the first year (no additional data were available during the second year for further comparison over time).

Table 2- Average LTE data obtained for concrete with low cement content (Cell 138)

Test Date	Slab ID	Approach Traffic		Departure Traffic	
		Inside	Outside	Inside	Outside
09/06/2017	4	86.7	90.6	86.0	94.4
	7	87.2	90.2	89.5	90.7
	11	89.5	92.4	94.8	97.1
	14	87.8	91.0	89.2	89.5
10/24/2017	4	91.7	92.4	90.5	92.7
	7	90.4	91.4	88.6	90.6
	11	96.0	93.0	92.5	92.1
	14	92.6	88.4	87.8	93.1
03/27/2018	4	79.1	87.2	83.2	87.6
	7	86.4	83.8	80.5	83.7
	11	90.0	81.6	87.0	82.8
	14	89.0	82.7	84.9	84.6
Average	4	85.8	90.1	86.6	91.6
	7	88.0	88.5	86.2	88.3
	11	91.8	89.0	91.4	90.7
	14	89.8	87.4	87.3	89.1

Table 3- Average LTE data obtained for concrete with lower cement content (Cell 238)

Test Date	Slab ID	Approach Traffic		Departure Traffic	
		Inside	Outside	Inside	Outside
09/06/2017	2	-	91.0	-	90.9
	6	92.8	88.3	96.7	90.0
	9	94.7	89.2	91.2	91.8
	13	86.9	90.9	95.7	89.9
10/24/2017	2	90.5	92.4	89.1	93.5
	6	90.7	91.4	89.8	91.3
	9	91.4	91.7	89.4	90.5
	13	91.0	94.1	89.2	92.9
03/27/2018	2	78.2	86.4	83.0	86.9
	6	88.7	85.1	85.7	83.6
	9	85.4	84.7	82.7	83.9
	13	83.0	87.2	82.3	84.2
Average	2	84.4	89.9	86.1	90.4
	6	90.7	88.3	90.7	88.3
	9	90.5	88.5	87.8	88.7
	13	87.0	90.7	89.1	89.0

Table 4- Average LTE data obtained for reference concrete (Cell 524)

Test Date	Slab ID	Approach Traffic		Departure Traffic	
		Inside	Outside	Inside	Outside
10/23/2017	2	92.9	89.0	91.4	84.5
	0	90.4	87.9	92.1	89.1
03/15/2018	2	87.1	75.0	87.7	77.4
	0	77.9	77.7	75.7	80.9
05/04/2018	2	93.1	90.4	92.1	92.6
	0	89.6	91.5	87.8	95.1
Average	2	91.0	84.8	90.4	84.8
	0	86.0	85.7	85.2	88.4

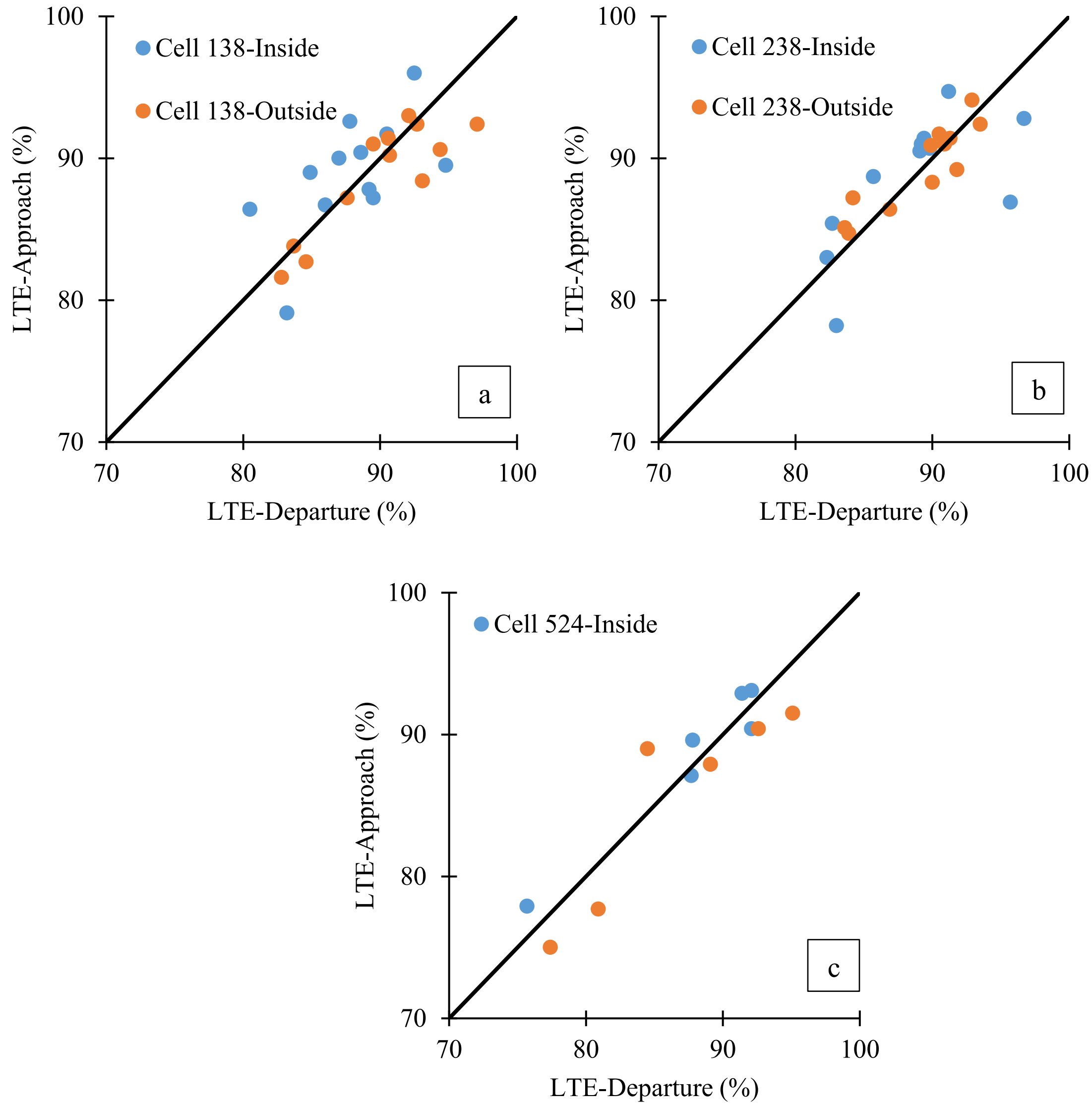

Figure 4- Variation in LTE as a function of traffic direction for low cement concrete (a), concrete with lower cementitious content (b), and reference mixture (c)

Data obtained from testing the slab at interior positions were employed for determining the modulus of subgrade reaction (K) values for the investigated panels according to AASHTO (1993). The area of deflection basin corresponding to 9000 lb loading was initially calculated based on Equation 2 (AASHTO 1993):

$$AREA = 6 \times \left[1 + 2\left(\frac{\delta_{12}}{\delta_0}\right) + 2\left(\frac{\delta_{24}}{\delta_0}\right) + \left(\frac{\delta_{36}}{\delta_0}\right)\right] \quad (2)$$

where δ_0 is the deflection in the center of loading plate (mm), δ_{12} is the deflection at 12 inches from the plate center (mm), δ_{24} is the deflection at 24 inches from the plate center (mm), and δ_{36} is the deflection at 36 inches from the plate center (mm).

Figure 5 proposed by AASHTO (1993) was then used for calculation of the dynamic K-value based on the calculated AREA and deflection at the center of the loading plate (mils).

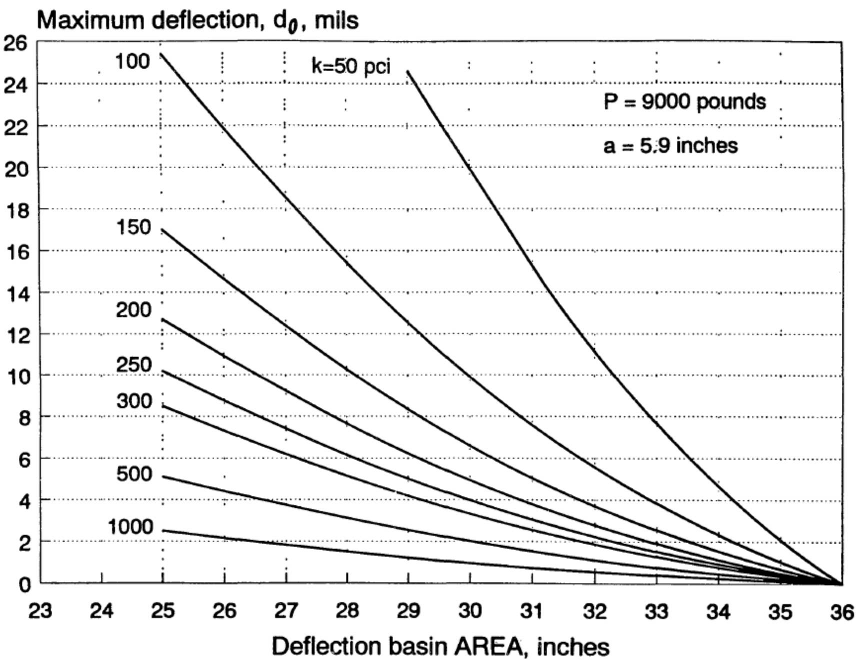

Figure 5- Dynamic k-value as a function of AREA and deflection at the center of the loading plate, borrowed from AASHTO (1993)

Table 5 summarizes the dynamic k-values obtained for the investigated slabs at different testing times obtained for center, corner, and mid-edge of the slabs at inside and outside lanes. The values reported in this table will serve as reference for over-time monitoring the subgrade performance.

In general the k-values were higher for the pavement cast with the reference concrete, indicating better preparation of the subgrade materials. It should be noted that the Cell 524 has a sand subgrade versus a clay/loam subgrade for Cells 138 and 238. Moreover, test results obtained for the reference cell (Cell 524) are affected by the lower slab thickness of 6.0 in. compared to 8.0 in. for Cells 138 and 238.

Table 5- Average dynamic k-values (psi)

Cell	Spot	Slab	Test Date							
			09/06/17	09/14/17	10/23/17	10/24/17	03/15/18	03/27/18	05/03/18	05/04/18
138	Center	4	200	-	-	180	-	350	148	-
		7	168	-	-	195	-	363	150	-
		11	178	-	-	163	-	235	175	-
		14	160	-	-	150	-	285	148	-
238		2	165	-	-	163	-	270	153	-
		6	180	-	-	183	-	370	158	-
		9	168	-	-	175	-	243	158	-
		13	148	-	-	135	-	265	140	-
524		0	-	378	250	-	253	-	-	290
		2	-	315	233	-	250	-	-	265
138	Corner	4	143	-	-	163	-	155	-	-
		7	155	-	-	138	-	150	-	-
		11	135	-	-	130	-	158	-	-
		14	143	-	-	138	-	150	-	-
238		2	138	-	-	166	-	160	-	-
		6	140	-	-	138	-	150	-	-
		9	130	-	-	145	-	160	-	-
		13	140	-	-	158	-	153	-	-
524		0	-	-	-	-	230	-	-	150
		2	-	-	-	-	205	-	-	143
138	Mid-edge	4	100	-	-	83	-	130	-	-
		7	80	-	-	83	-	105	-	-
		11	113	-	-	88	-	108	-	-
		14	93	-	-	83	-	123	-	-
238		2	80	-	-	98	-	108	-	-
		6	83	-	-	75	-	113	-	-
		9	75	-	-	85	-	105	-	-
		13	80	-	-	80	-	75	-	-
524		0	-	-	98	-	190	-	-	120
		2	-	-	88	-	165	-	-	105

Ride Quality

MnDOT's Lightweight Profiler, conforming to ASTM E-950 requirements (Figure 6) was used for collection of the ride quality data in terms of the International Roughness Index (IRI) according to the following timeline:

Reference Concrete (Cell 524): testing was performed on 10/26/2017, 03/28/2018, 04/25/2018, 06/11/2018, 08/16/2018, and 10/02/2018 on both the inside and outside traffic lanes

Low Cement Concrete (Cell 138): testing was performed on 07/18/2017, 07/20/2017, 07/25/2017, 11/03/2017, 11/30/2017, 03/28/2018, 04/23/2018, 05/31/2018, 06/14/2018, 07/09/2018, 07/26/2018, 08/16/2018, and 10/02/2018 on both the inside and outside traffic lanes

Lower Cement Concrete (Cell 238): testing was performed on 07/18/2017, 07/20/2017, 07/25/2017, 11/03/2017, 11/30/2017, 03/28/2018, 04/23/2018, 05/31/2018, 06/14/2018, 07/09/2018, 07/26/2018, 08/16/2018, and 10/02/2018 on both the inside and outside traffic lanes

Figure 6- MnDOT's Lightweight Profiler

Tables 6-8 summarize the IRI data obtained for the investigated pavement. The reported data are the average of three IRI readings from both the right and left wheel tracks, along with the corresponding Mean Roughness Index (MRI) values. Figure 7 also presents the variation in MRI values over time, for both the inside and outside lanes of the investigated cells during the first two years.

Comparable performance was observed for the Cells 138 and 238 for the first two years. The MRI values obtained for the outside lane were generally lower than the ones recorded for the inside lane (exposed to traffic) at Cell 138. Trends were reversed for Cell 238, with higher MRI values obtained for the outside lane. The minimum MRI values were recorded during the first month from construction with values limited to 108 in./mile for both cells. However, an increase in MRI was observed for the measurements taken during the period of November 2017 to October 2018. The increase in MRI was more pronounced for the inside lane which can be due to the exposure to traffic loading. The MRI values obtained for the inside lane ranged from 107 to 139, and from 86 to 110 in./mile for Cells 138 and 238, respectively.

The data obtained for inside lane of the reference cell (Cell 524) revealed consistent performance over time, with no significant difference between measurements performed in October 2017 and the ones taken in October 2018. The MRI values obtained for the outside lane of Cell 524 were constantly higher than those obtained for the inside lane which is exposed to controlled traffic loading.

MRI values observed for Cell 524 seem to be slightly lower than those observed in cells 138 and 238. One should also consider the difference in thickness of the investigated pavements, where the reference cell is 6.0 in. thick, compared to 8.0-in. thick pavement at Cells 138 and 238.

It should be noted that a MRI of no more than 65 in./mile is typically recommended by MNDOT. Given the short length of the test cells, such low IRI values are hard to achieve during paving. However, the presented data will only serve as the baseline for comparing the performance of the low cement pavement sections over time. Further data will be available for future annual cell performance reports.

Table 6- Ride quality data for Cell 524

Concrete Type	Test Date	Lane	Wheel path	IRI (in./mile)	MRI (in./mile)
Reference; Cell 524	10/26/2017	Inside	Left	93.2	99.1
			Right	105.0	
		Outside	Left	101.1	108.1
			Right	115.1	
	03/28/2018	Inside	Left	84.4	89.2
			Right	94.0	
		Outside	Left	93.2	101.2
			Right	109.2	
	04/25/2018	Inside	Left	81.1	85.0
			Right	88.8	
		Outside	Left	85.2	90.6
			Right	96.0	
	06/11/2018	Inside	Left	100.4	110.6
			Right	120.8	
		Outside	Left	109.7	115.9
			Right	122.1	
	08/16/2018	Inside	Left	85.0	89.1
			Right	93.3	
		Outside	Left	94.8	99.2
			Right	103.6	
	10/02/2018	Inside	Left	86.5	95.9
			Right	105.2	
		Outside	Left	96.3	102.3
			Right	108.3	

Table 7- Ride quality data for Cell 138

Concrete Type	Test Date	Lane	Wheel path	IRI (in./mile)	MRI (in./mile)
Low cement; Cell 138	07/18/2017	Inside	Left	112.7	108.1
			Right	103.5	
		Outside	Left	116.0	102.6
			Right	89.1	
	07/20/2017	Inside	Left	112.5	107.8
			Right	103.1	
		Outside	Left	115.7	102.2
			Right	88.6	
	07/25/2017	Inside	Left	114.5	106.9
			Right	99.2	
		Outside	Left	114.5	101.1
			Right	87.8	
	11/03/2017	Inside	Left	136.35	135.40
			Right	134.64	
		Outside	Left	86.11	88.70
			Right	91.49	
	11/30/2017	Inside	Left	134.13	137.49
			Right	140.98	
		Outside	Left	87.75	90.60
			Right	93.65	
	03/28/2018	Inside	Left	143.60	136.47
			Right	129.34	
		Outside	Left	126.98	114.52
			Right	102.06	
	04/23/2018	Inside	Left	129.22	120.39
			Right	111.55	
		Outside	Left	115.65	102.29
			Right	88.93	
	05/31/2018	Inside	Left	135.35	127.65
			Right	119.95	
		Outside	Left	112.82	101.10
			Right	89.38	
	06/14/2018	Inside	Left	120.45	124.38
			Right	128.37	
		Outside	Left	157.77	139.39

			Right	121.52	
	07/09/2018	Inside	Left	116.84	106.89
			Right	96.75	
		Outside	Left	109.87	110.25
			Right	110.56	
	07/26/2018	Inside	Left	141.80	139.39
			Right	136.79	
		Outside	Left	107.97	100.93
			Right	93.96	
	08/16/2018	Inside	Left	128.95	122.91
			Right	116.88	
		Outside	Left	118.67	104.13
			Right	89.58	
	10/02/2018	Inside	Left	136.94	129.83
			Right	122.72	
		Outside	Left	117.09	105.71
			Right	94.33	

Table 8- Ride quality data for Cell 238

Concrete Type	Test Date	Lane	Wheel path	IRI (in./mile)	MRI (in./mile)
Low cement; Cell 238	07/18/2017	Inside	Left	100.8	89.6
			Right	78.5	
		Outside	Left	97.7	104.3
			Right	111.0	
	07/20/2017	Inside	Left	100.8	89.7
			Right	78.6	
		Outside	Left	100.8	105.0
			Right	109.2	
	07/25/2017	Inside	Left	98.2	87.1
			Right	75.9	
		Outside	Left	100.8	104.5
			Right	108.2	
	11/03/2017	Inside	Left	93.52	86.80
			Right	80.09	
		Outside	Left	124.63	133.50
			Right	142.12	
	11/30/2017	Inside	Left	118.48	110.44
			Right	102.45	
		Outside	Left	125.01	132.61
			Right	140.47	
	03/28/2018	Inside	Left	109.40	103.06
			Right	96.72	
		Outside	Left	105.82	111.47
			Right	117.11	
	04/23/2018	Inside	Left	99.14	90.00
			Right	80.85	
		Outside	Left	99.10	104.45
			Right	109.80	
	05/31/2018	Inside	Left	100.24	90.93
			Right	81.61	
		Outside	Left	102.51	105.00
			Right	107.49	
	06/14/2018	Inside	Left	116.77	110.25
			Right	103.66	
		Outside	Left	90.54	94.41

			Right	98.71	
	07/09/2018	Inside	Left	93.58	87.88
			Right	82.37	
		Outside	Left	114.30	115.13
			Right	115.57	
	07/26/2018	Inside	Left	104.42	94.85
			Right	85.22	
		Outside	Left	129.63	133.69
			Right	137.55	
	08/16/2018	Inside	Left	104.94	95.63
			Right	86.32	
		Outside	Left	97.00	103.99
			Right	110.99	
	10/02/2018	Inside	Left	101.21	92.96
			Right	84.71	
		Outside	Left	106.40	111.70
			Right	117.01	

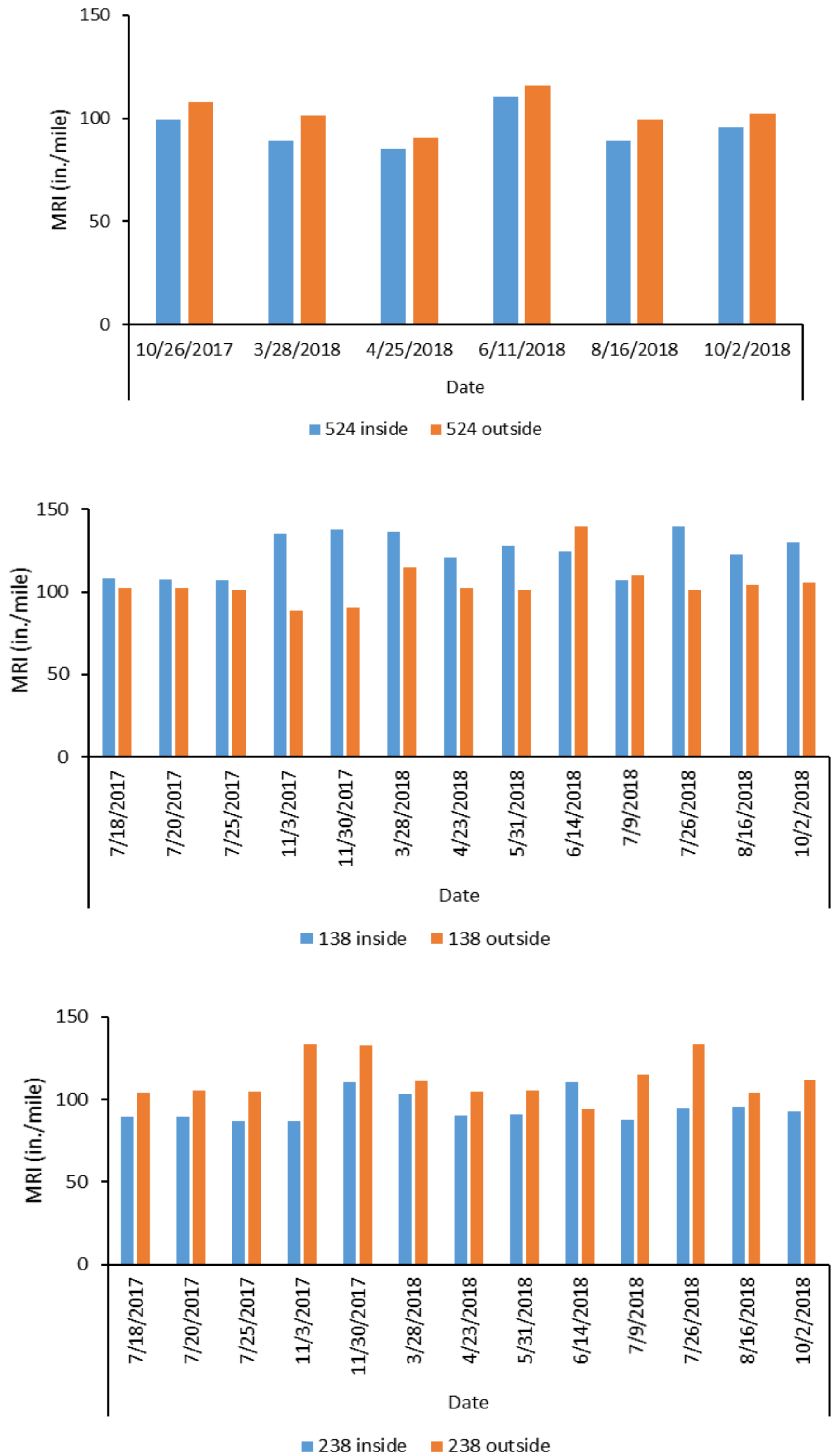

Figure 7- Variation in MRI (in./mile) values as a function of time

Dynamic Load Test

A 5-axle, 18-wheel semi-tractor trailer with total weight of 80 kips was used for loading the pavement sections. Figure 8 offers a schematic view of the vehicle configurations. Table 9 summarizes the axle loads. Testing was conducted on pavement cast with low and lower cement content on 09/13/2017, 03/21/2018, 05/02/2018, 07/31/2018, and 10/31/2018. The loading was conducted at two speed levels of 5 and 35 mph, replicated five times per speed scenario. For each pavement type, response to the dynamic lading was recorded by 8 sensors, installed at different depths and locations as detailed in Figure 9. The CE sensors measure the dynamic strain gages and VWs are the vibrating wire strain gages. The investigated sensors were located at top and bottom of the slabs, at both the corner and mid-edge spots of the instrumented panels, as detailed in Table 10 and Table 11.

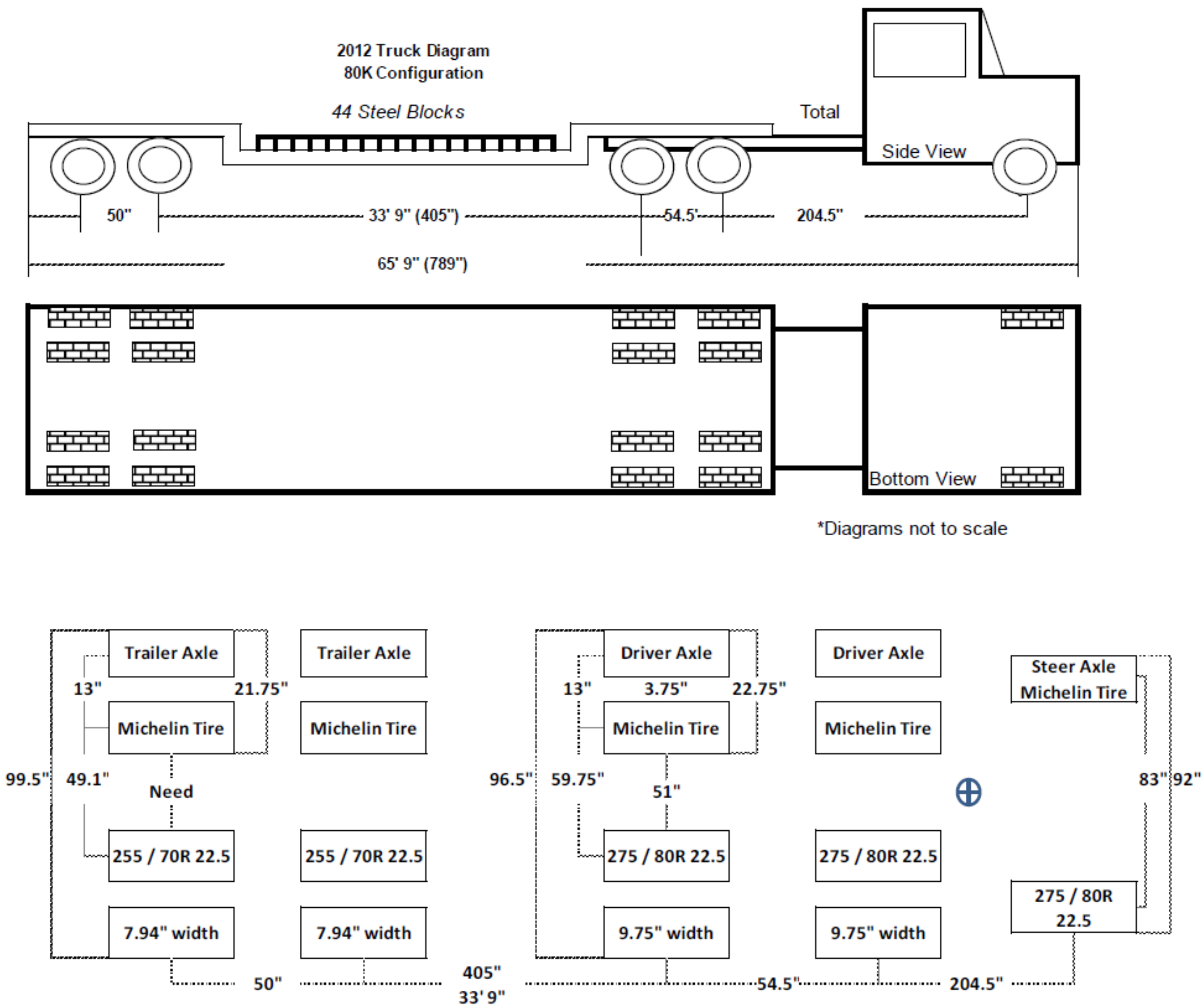

Figure 8- Vehicle dimensions and axle configurations for the Workstar truck and the Towmaster trailer employed for dynamic loading (MnDOT 2013)

Table 9- Axle weight for the Workstar truck and the Towmaster trailer employed for dynamic loading (MnDOT 2013)

	Tractor	**Tractor Tandem**		**Trailer Tandem**	
Total Weight	Steering Axle	Front Axle	Back Axle	Front Axle	Back Axle
79,700	11,700	17,650	16,450	16,800	17,100
		34,100		33,900	

Figure 9- Sensor installation plan for Cell 138 (top) and Cell 238 (bottom).

Table 10- As-built location of sensors installed in mixtures prepared with low and lower cementitious materials content

Cell 138				Cell 238			
Sensor #	**Station**	**Offset (ft)**	**Depth (in.)**	**Sensor #**	**Station**	**Offset (ft)**	**Depth (in.)**
CE001	9353.95	11.2	0.8	CE001	9474.07	10.9	0.8
CE002	9353.95	11.2	7.5	CE002	9474.07	10.9	7.5
CE003	9360.01	11.0	0.8	CE003	9480.08	10.9	0.8
CE004	9360.01	11.0	7.5	CE004	9480.08	10.9	7.5
CE005	9368.98	10.8	0.8	CE005	9489.07	10.9	0.8
CE006	9368.98	10.8	7.5	CE006	9489.07	10.9	7.5
CE007	9374.97	10.8	0.8	CE007	9495.02	11.1	0.8
CE008	9374.97	10.8	7.5	CE008	9495.02	11.1	7.5

Table 11- Detailed layout of the sensors embedded in Cell 138 and Cell 238

<table>
<tr><th colspan="4">Cell 138 & 238</th></tr>
<tr><th>Location in Slab</th><th>Depth</th><th>Orientation</th><th>Sensor #</th></tr>
<tr><td rowspan="4">Corner</td><td rowspan="2">Top</td><td>Transverse</td><td>CE001</td></tr>
<tr><td>Transverse</td><td>CE005</td></tr>
<tr><td rowspan="2">Bot.</td><td>Transverse</td><td>CE002</td></tr>
<tr><td>Transverse</td><td>CE006</td></tr>
<tr><td rowspan="4">Mid-Edge</td><td rowspan="2">Top</td><td>Longitudinal</td><td>CE003</td></tr>
<tr><td>Longitudinal</td><td>CE007</td></tr>
<tr><td rowspan="2">Bot.</td><td>Longitudinal</td><td>CE004</td></tr>
<tr><td>Longitudinal</td><td>CE008</td></tr>
</table>

Data was recorded with a frequency of 1200 Hz. The total test time was about 5 and 20 s for loading at 35 and 5 mph, respectively. The average of readings obtained through first 2 and 0.5 seconds were calculated and employed as the base line for normalizing the data for 5 and 35 mph scenarios, respectively. Figure 10 presents an example of traffic loading data obtained from Sensor # CE008, located at bottom part, mid-edge of Cell 238. Given the high frequency of data recording, trend lines were employed for further clarification of the load-deflection patterns as shown in Figure 10. Note that the scattered blue lines are the normalized raw data and the trend line is shown in yellow, which clearly depicts the local maxima under the front wheel and the rear tandem axels.

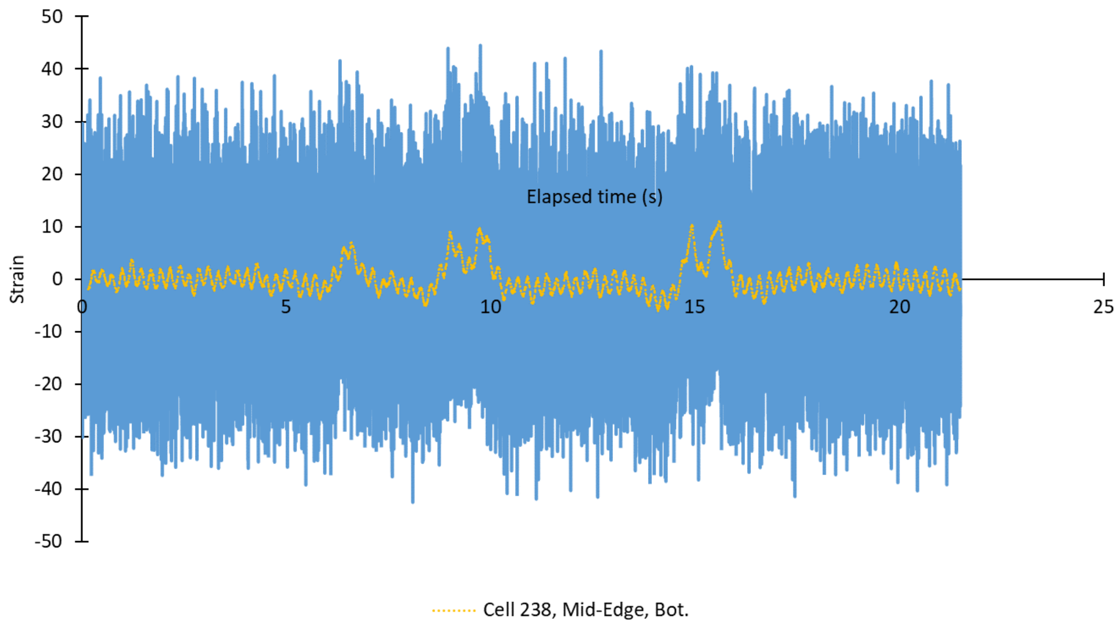

Figure 10- Sample raw data and corresponding trend line obtained from dynamic load test

Figure 11 and Figure 12 present the trend lines observed for sensors embedded at different depths and different spots of pavements made with low and lower cementitious materials content. Change in direction of stress was observed with the load moving on the pavement surfaces. Trends were similar for the data obtained from both cells cast with Low or Lower cementitious materials content. Results indicate similar performance for the two sensors located at the same depth and the same spot of the panels within the same concrete type. Comparable responses were obtained for loading the pavement at 5 and 35 mph, for a given combination of test spot, sensor depth, and concrete type. However, deformations were higher for the sensors located at mid-edge compared to those located at corner of the slabs. Moreover, the sensors embedded at bottom and top of the mid-edge spots exhibited more symmetrical data, corresponding to compressive and tensile strains (and stresses) induced by the moving truck.

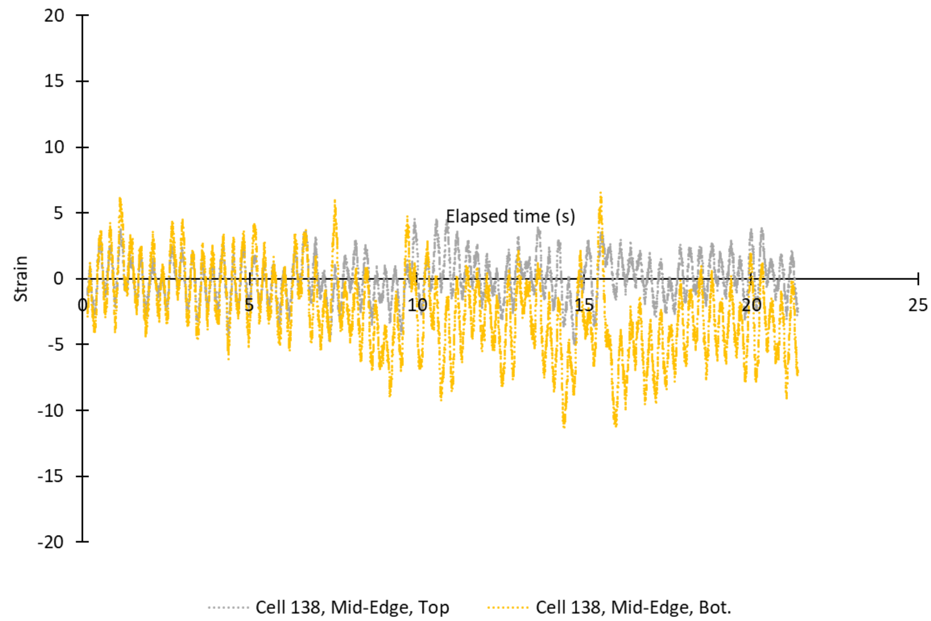

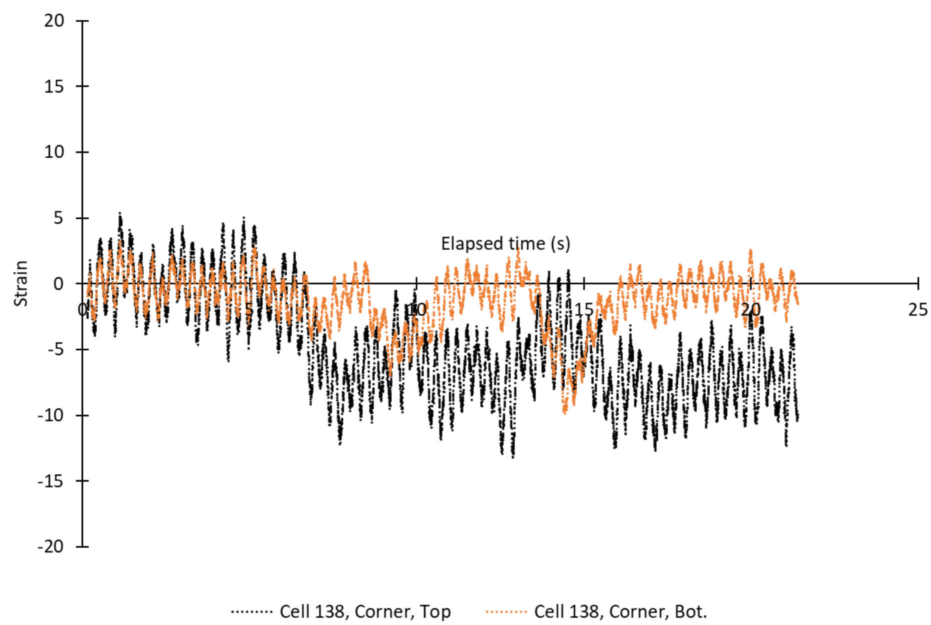

Figure 11- Load-deflection patterns for Cell 138 at corner and mid-edge

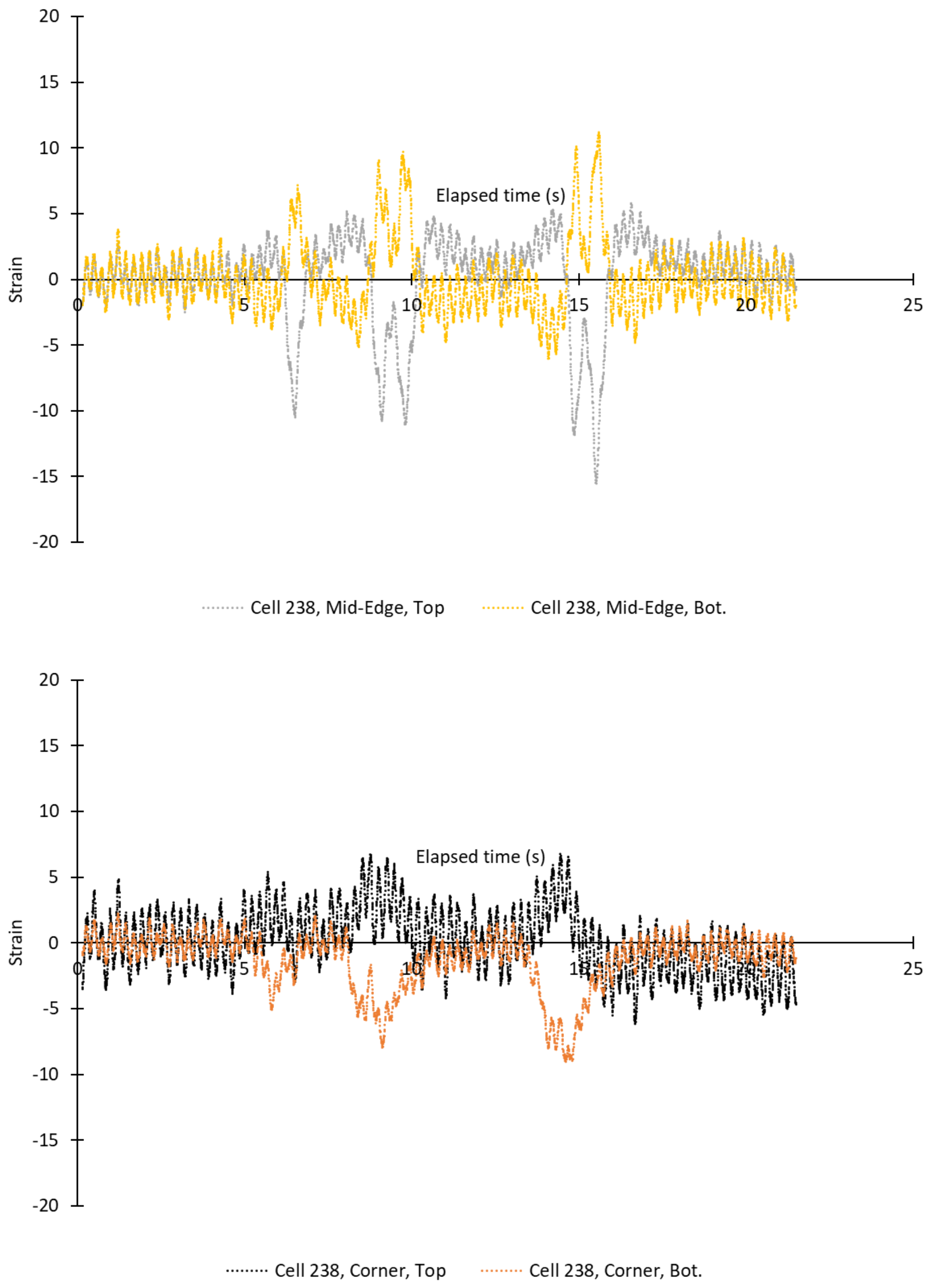

Figure 12- Load-deflection patterns for Cell 238 at corner and mid-edge

Table 12 summarizes the minimum and maximum strain values obtained for sensors located at top and bottom parts of the investigated panels. The values reported in this table are the average of five sets of readings per scenario. It should be noted that even though the loading test was performed five times for each section, the first sets of measurements yielded significantly lower strain values in almost all test scenarios. Therefore, the presented data are the average values for four measurements conducted at 5 and 35 mph. Moreover, the reported values were not corrected for traffic wander.

The values reported in this table are high for an 8.0 in. thick pavement. But this can be in part due to the noise in recording the data. The maximum and minimum strain values were comparable for both concrete types and did not follow a constant pattern favoring a certain mixture. In other words, the variation in cementitious materials content did not have a significant effect on registered maximum and minimum values and the investigated cells exhibited comparable response to traffic loading. This was in line with the comparable load-deflection patterns obtained for the mixtures presented in Figure 11 and Figure 12. It should be noted that some of the CE sensors did not respond to the dynamic loading conducted on 07/31/2018 and 10/31/2018. This was reflected in Table 12.

Table 12- Summary of the Max. and Min. strain values obtained through different testing scenarios for sensors embedded in Cell 138 and Cell 238

Cell #				**138**				**238**			
Location on Slab				**Corner**		**Mid-Edge**		**Corner**		**Mid-Edge**	
Depth				**Top**	**Bot.**	**Top**	**Bot.**	**Top**	**Bot.**	**Top**	**Bot.**
5 mph	09/13/2017	Avg.	Min.	-104	-59	-110	-60	-117	-54	-133	-55
			Max.	46	37	41	49	43	27	34	42
		Std.	Min.	7	6	8	8	17	5	4	10
			Max.	3	3	2	4	3	1	1	1
	03/21/2018	Avg.	Min.	-157	-62	-170	-70	-92	-42	-92	-50
			Max.	61	54	50	66	52	32	37	49
		Std.	Min.	4	8	7	8	29	6	31	6
			Max.	1	1	1	4	1	1	3	4
	05/02/2018	Avg.	Min.	-121	-55	-126	-57	-137	-53	-151	-56
			Max.	32	28	31	36	69	35	42	62
		Std.	Min.	17	7	16	6	12	3	11	1
			Max.	1	0	2	1	4	2	4	7
	07/31/2018	Avg.	Min.	-171	-93	-121	-172	-89	-57	NA	-61
			Max.	124	82	102	121	45	30	NA	41
		Std.	Min.	30	7	27	27	23	15	NA	10
			Max.	16	11	9	18	4	1	NA	3
	10/31/2018	Avg.	Min.	-279	-160	NA	-242	-151	NA	NA	-120
			Max.	279	162	NA	246	113	NA	NA	117
		Std.	Min.	12	9	NA	7	71	NA	NA	7
			Max.	12	4	NA	12	42	NA	NA	5
35 mph	09/13/2017	Avg.	Min.	-104	-56	-109	-61	-129	-59	-132	-67
			Max.	40	33	35	40	35	22	28	33
		Std.	Min.	14	8	11	12	7	6	4	4
			Max.	3	2	3	2	3	2	2	1

	03/21/2018	Avg.	Min.	-155	-65	-168	-76	-102	-52	-109	-54
			Max.	57	51	48	62	50	29	32	42
		Std.	Min.	22	15	19	14	18	11	9	12
			Max.	4	4	2	3	12	2	2	6
	05/02/2018	Avg.	Min.	-142	-73	-149	-84	-152	-58	-159	-67
			Max.	69	52	54	76	61	32	37	51
		Std.	Min.	12	6	9	6	20	13	16	18
			Max.	5	5	1	6	6	2	2	4
	07/31/2018	Avg.	Min.	-115	-74	-148	-95	-118	-55	NA	-69
			Max.	101	64	91	94	36	26	NA	36
		Std.	Min.	17	15	56	5	6	4	NA	11
			Max.	3	3	10	5	0	0	NA	2
	10/31/2018	Avg.	Min.	-253	-142	NA	-219	-131	NA	NA	-103
			Max.	263	149	NA	228	125	NA	NA	105
		Std.	Min.	20	8	NA	20	12	NA	NA	8
			Max.	23	13	NA	19	11	NA	NA	9

*No reliable sensor data were available

In-Situ Static Deformation

Vibrating wire strain gages (VWSG) embedded at corner and mid-panel areas were used to monitor the total in-situ deformations due to environmental loads.

Cell 138				**Cell 238**			
Sensor #	**Station**	**Offset (ft)**	**Depth (in.)**	**Sensor #**	**Station**	**Offset (ft)**	**Depth (in.)**
VW001	9384.13	11.0	0.8	VW001	9459.00	10.9	0.8
VW002	9384.13	11.0	7.5	VW002	9459.00	10.9	7.5
VW003	9390.16	6.0	0.8	VW003	9464.98	6.0	0.8
VW004	9390.16	6.0	7.5	VW004	9464.98	6.0	7.5

The recorded deformations were caused by a combination of concrete shrinkage, warping due to moisture loss, curling due to temperature gradient within the depth of concrete, and linear deformation of the sensors and the surrounding concrete due to variations in temperature.

The raw frequency data recorded by the VWSGs were converted to iso-thermal strain values as instructed by Equations 3 and 4 (MnDOT 2013).

$$S = FW^2 \times D \tag{3}$$

$$\varepsilon_{iso-thermal} = (S_1 - S_0) + [(T_1 - T_0) \times (\alpha_{st} - \alpha_c)] \tag{4}$$

where S is the value of strain calculated based on vibration frequency (με), FW is the vibration frequency registered by the VWSG (Hz), D is the gage factor equal to 0.003304, $\varepsilon_{iso-thermal}$ is the iso-thermal concrete strain (με), S_1 is the strain (με) at temperature T_1 (°C), S_0 is the strain (με) corresponding to baseline measurement at baseline temperature T_0 (°C), and α_{st} is the coefficient of thermal expansion of steel equal to 12 in./in./°C, and α_c is the coeffiecint of thermal expansion of concrete equal to 9 in./in./°C as reported in the first year performance report.

Figure 14 presents the strain history and temperature data recorded during the first two years from casting the cells. Time zero readings correspond to the strain values at the time of placing the concrete. For both mixtures, VWSG 1 and VWSG 3 present the deformations close to the surface of the concrete, at corner and mid-panel, respectively, while VWSG 2 and VWSG 4 present the deformations at bottom part of the concrete, at corner and mid-panel, respectively. VWSG 1 and VWSG 2 had transverse orientation, while VWSG 3 and VWSG 4 were oriented longitudinally.

In general, the investigated sensors exhibited similar deformation pattern, with a tendency towards negative strain values, corresponding to compressive stresses. The sensors located at top parts of the pavement exhibited higher values compared to the ones placed at bottom part of the pavement. The sensors with longitudinal orientation generally exhibited higher strain values compared to the traverse direction at same depth. The strain values obtained for Cell 138 cast with low cementitious materials were higher than the corresponding values at Cell 238 with lower cementitious materials content.

A range of 45°C was observed for the variations in seasonal temperature as presented in Figure 13 and Figure 14. However, such cyclic variations were not exactly reflected in total strain values. This highlights the fact that other factors, including shrinkage and/or warping in light of moisture gradient in depth governed the deformations.

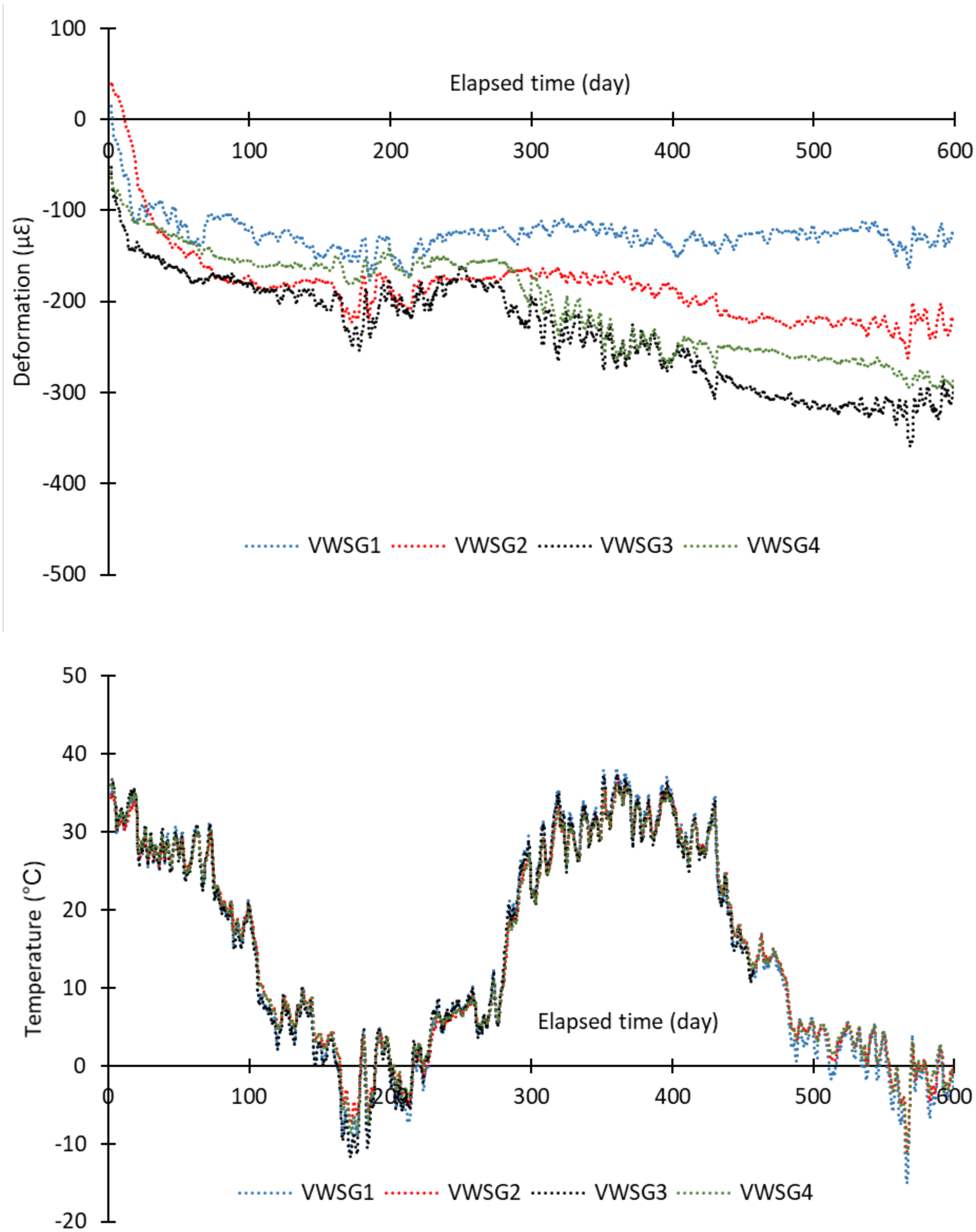

Figure 13- Iso-thermal in-situ deformation (με) for Cell 138 (top) and corresponding temperature readings (bot.)

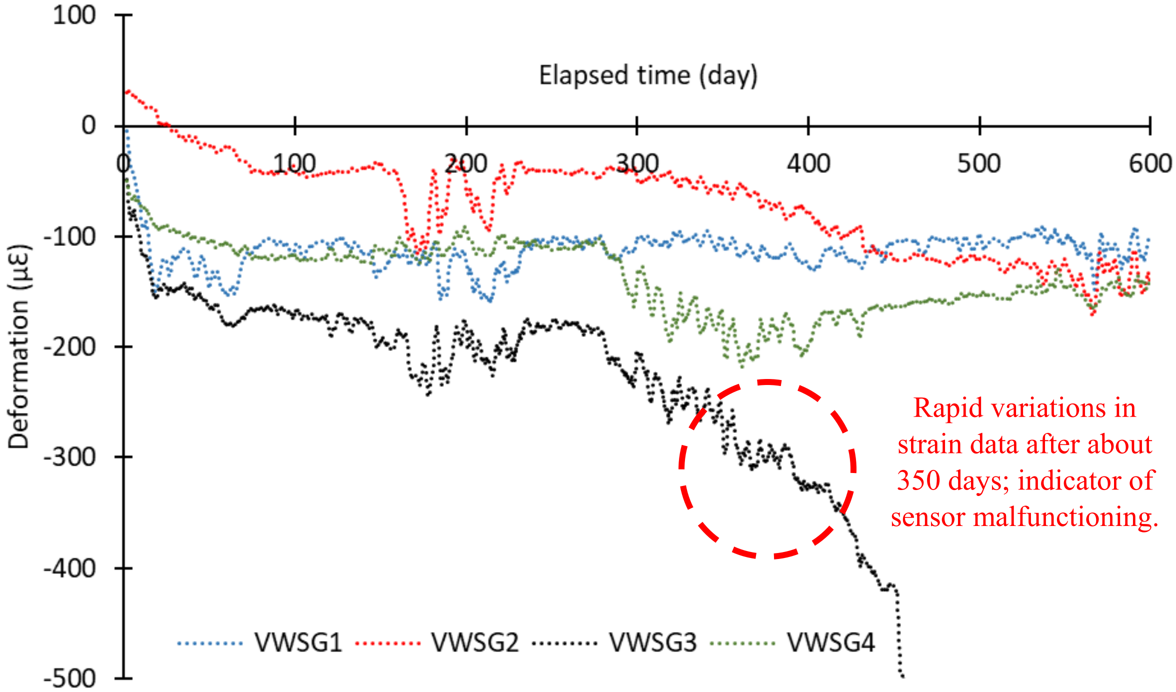

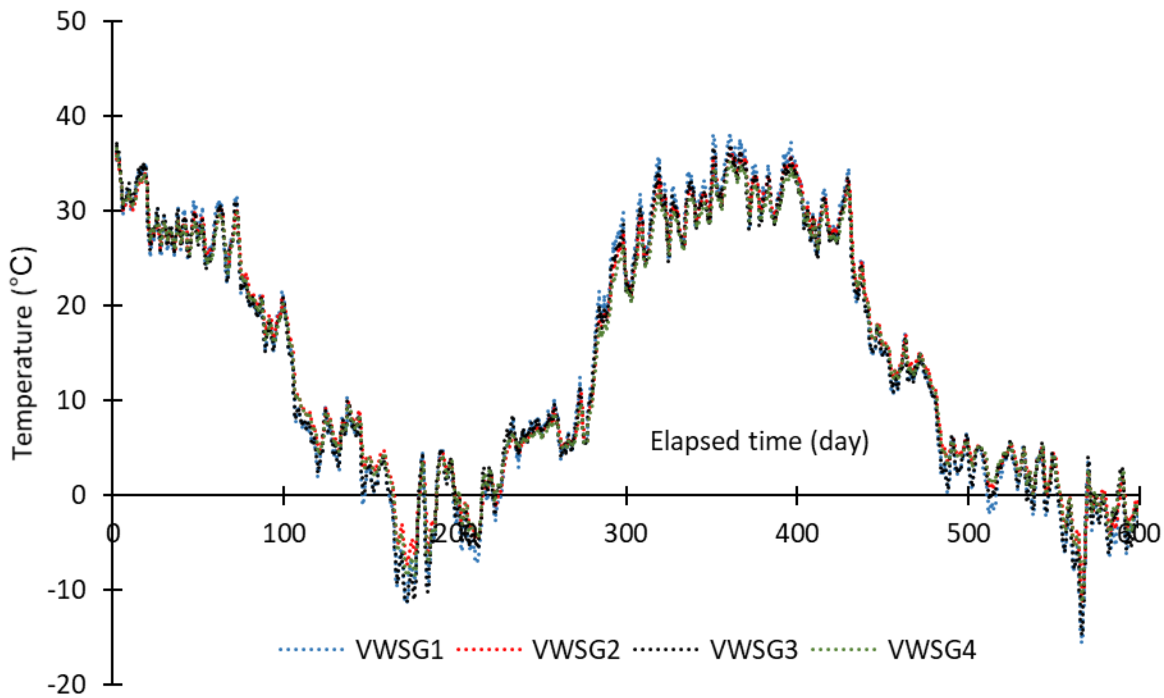

Figure 14- Iso-thermal in-situ deformation (με) for Cell 238 (top) and corresponding temperature readings (bot.)

Temperature of pavement structure

Thermocouple trees were employed for monitoring the temperature variations within the depth of pavement structure, including the concrete slab and the base layer. Table 13 offers a summary of placement details for thermocouples incorporated at different spots in Cell 138. Data obtained from sensors embedded in Station 9396.13 (TC#1 to TC#8) are presented in this section. Data obtained from sensors embedded in Station 9390.8 (TC#9 to TC#20) are presented in the Appendix.

Table 13- Placement details for thermocouples in Cell 138

Station	Offset (ft)	TC #	Depth from surface (in.)	Surrounding material
9396.13	-11.44	1	0.5	Concrete
		2	1	Concrete
		3	4	Concrete
		4	7.5	Concrete
		5	8.5	Gravel
		6	10.5	Gravel
		7	12	Gravel
		8	14	Clay
9390.8	-6.17	9	0.5	Concrete
		10	1	Concrete
		11	4	Concrete
		12	7.5	Concrete
		13	8.5	Gravel
		14	12	Gravel
		15	14	Clay
		16	24	Clay
		17	36	Clay
		18	48	Clay
		19	60	Clay
		20	72	Clay

Figure 15 presents the trend lines obtained for variations in temperature at different depths of concrete slab at Cell 138. Trend lines were employed to avoid the wide scatter in data, thus making it easier to follow the trends. Results indicated uniform patterns in temperature fluctuations regardless of the depth. Data obtained for thermocouples were similar to temperature data recorded by the VWSGs shown in Figure 13 and Figure 14.

The actual temperature measurements at top and bottom of pavement are presented in Figure 16. Data indicates a wider range of short- and long-term variations in temperature reading at top part of the pavement while compared to the depth of the slab. Figure 17 presents the extent of variation in temperature between top and bottom part of the concrete slab. The black line is the trend line, exhibiting higher temperatures at surface during the warmer seasons and higher temperatures at bottom of the slab during the cold seasons. The blue line is the actual data, exhibiting up to 15°C temperature difference between top surface and bottom during the cold season. This corresponds to a gradient of over 2°C/in. (3.6 °F/in.) within the depth of the slab.

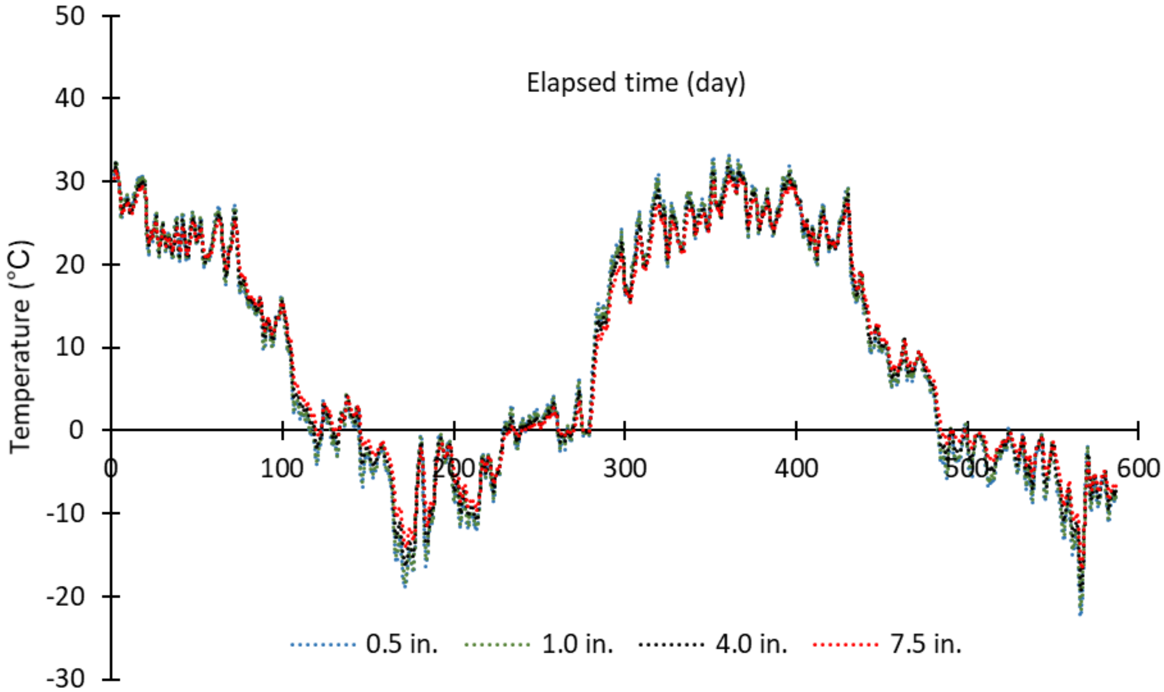

Figure 15- Temperature variations at different depths of concrete slab in Cell 138

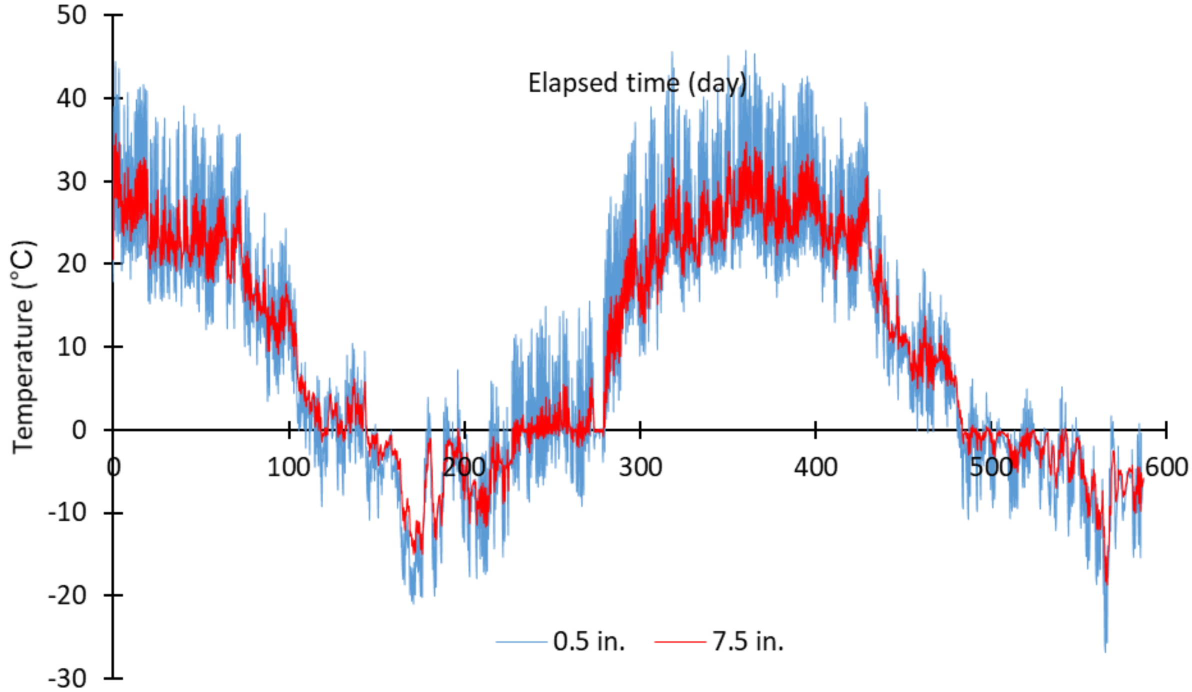

Figure 16- Temperature readings at top (0.5 in.) and bottom (7.5 in.) of concrete slab in Cell 138

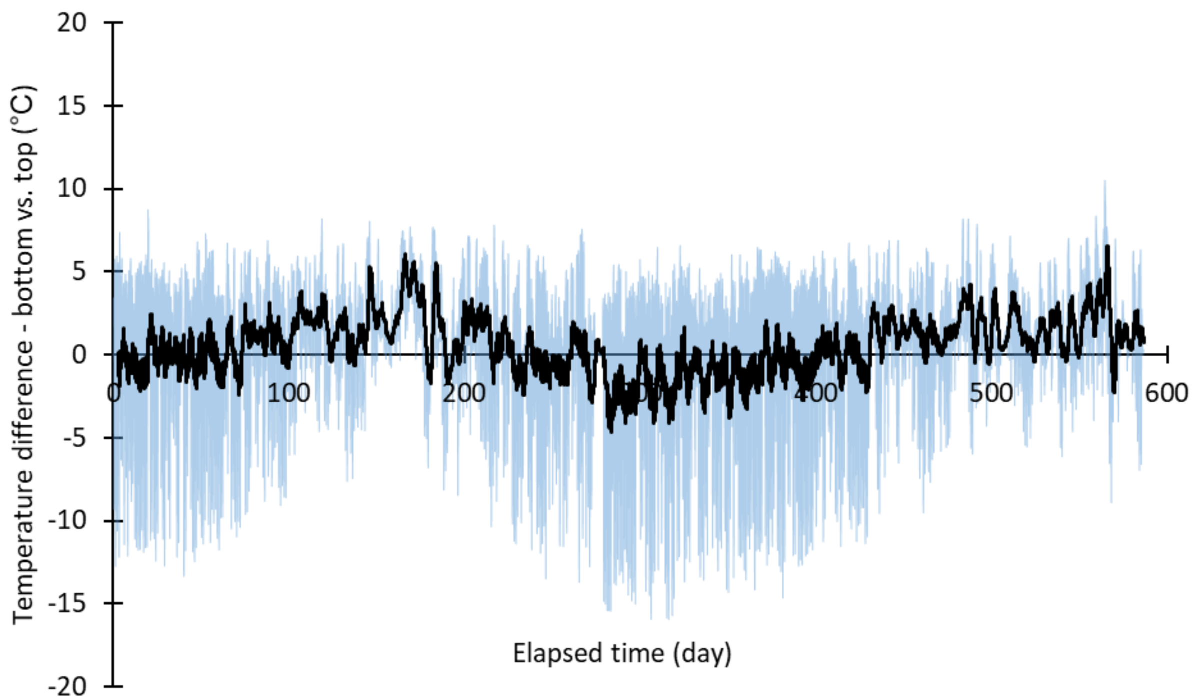

Figure 17- Temperature variations between the top and bottom of concrete slab in Cell 138

Temperature profile underneath the concrete slab is presented in Figure 18. Trends were comparable to those observed for the concrete slab, with lower variations between the maximum and minimum values. It is worth mentioning that the base layer experienced freezing conditions in over 130 days within the first year.

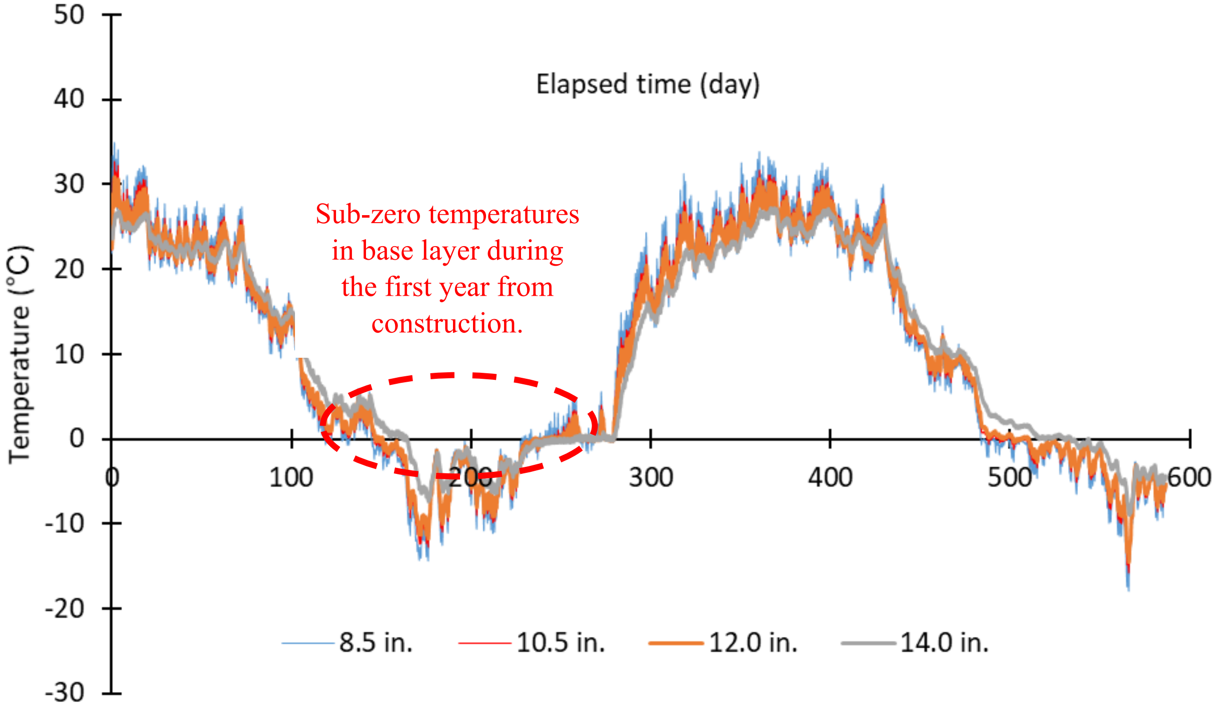

Figure 18- Temperature variations at base layer underneath the concrete slab in Cell 138

Moisture in pavement structure

Decagon 5TE sensors were employed for monitoring the variations in moisture content within the depth of pavement structure, including the concrete slab and the base layer. Table 14 offers a summary of placement details for 5TE sensors incorporated at different spots in Cell 138 as presented in the construction report.

Table 14- Placement details for 5TE sensors in Cell 138

Sensor ID	Station	Offset (ft)	Depth (in.)	Surrounding material
EC001	9390.73	-5.69	1.0	Concrete
EC002	9390.73	-5.69	4.0	Concrete
EC003	9389.90	-6.01	12.0	Class 5 aggregate
EC004	9389.90	-6.01	24.0	Clay
EC005	9389.90	-6.01	30.0	Clay

No calibration equation is curently available to convert the raw data to VWC for the sensors embedded in concrete. The EW data obtained for EC001 and EC002 (EW1 and EW2) were not included in this section. Data are available in Appendix. Calibration as presented in Equations 5 and 6 (MnDOT 2013) was considered to determine the volumetric water content (VWC) based on the raw data for sensors embeded in Class 5 aggregate base and clay subgarde, respectively:

$$VWC_{Class\ 5} = 0.0003 \times EW - 0.0239 \tag{5}$$

$$VWC_{Clay} = 0.0003 \times EW - 0.0021 \tag{6}$$

Figure 19 presents the variations in VWC (%) for sensors embeded in the 5.0 in. thick layer of Class 5 aggregate base (EW3). This sensor is located at depth of 12.0 in. from pavement surface, which corresponds to 4.0 in. from underneath the concrete slab. Variation in base layer temperature at same depth (obtained from thermocouples) is also presented in Figure 20.

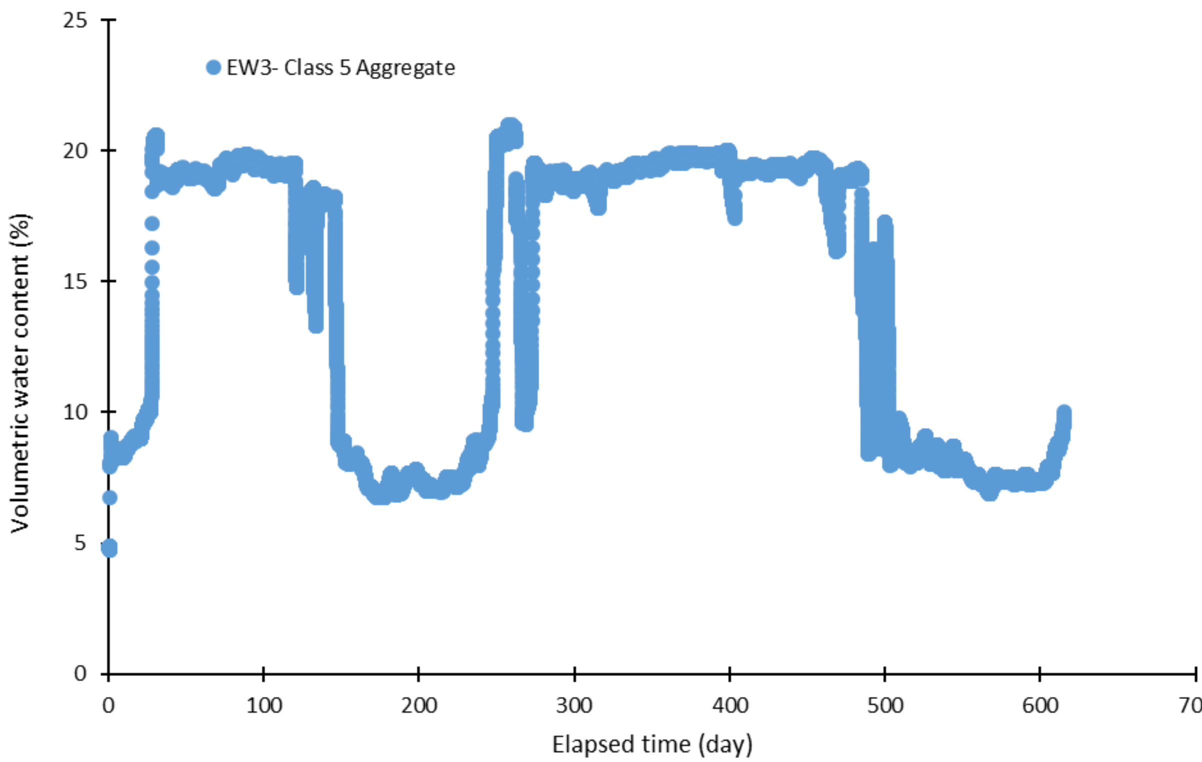

Figure 19- Variations in volumetric water content (%) at base layer underneath the concrete slab in Cell 138

Data presented in Figure 19 indicated VWC of 13% to 21% when the base layer is not frozen. VWC results exhibited a tendncy to drop to values as low as 6% to 8% when the base layer is exposed to subzero temperatures. Examples of this condition are observed for recordings between 150 and 250 days, as well as recordings between 500 and 600 days. Such transitions are sudden and can occure in a day or two. These observations are in agreement with temperature fluctuations presented in Figure 20.

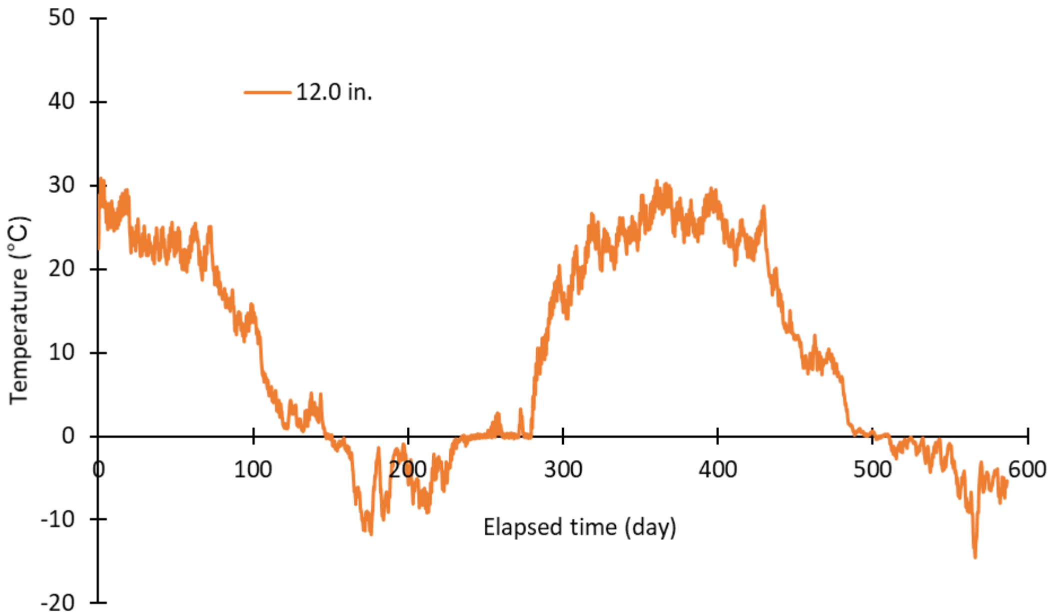

Figure 20- Thermocouple temperature readings at Class 5 aggregate base layer underneath the concrete slab in Cell 138

Trends were similar for the sensors embeded in the clay subgrade underneath Cell 138. However, higher VWC values were observed for the clay layer while compared to Class 5 aggregate. Data obtained for sensor embeded at 24.0 in. from surface, presented in Figure 21, indicated VWC of 30% to 37% when the base layer is not frozen. Again the VWC results exhibted a significant drop to values as low as 12% to 14% when the clay subgrade was exposed to freezing temperatures. For the sensors located in clay subgrade, such transitions occurred during a longer period of time (about 1-3 weeks).

Trends obtained for the 5TE sensor embeded at depth of 36 in. (presented with yellow color in Figure 21) were in general agreement with the data obtained at depth of 24.0 in. Lower VWC of 6-10% was observed at this depth for the freezing temperatures. Moreover, higher VWC of about 42% was observed at this depth during the period of 25 to 150 days. Such a trend was not observed for the period of 300 to 500 days. A sudden drop in VWC was recorded during this period of time. The reason for such an observation is not clear at this time, but sensor malfunctioning can be a reason for this observation.

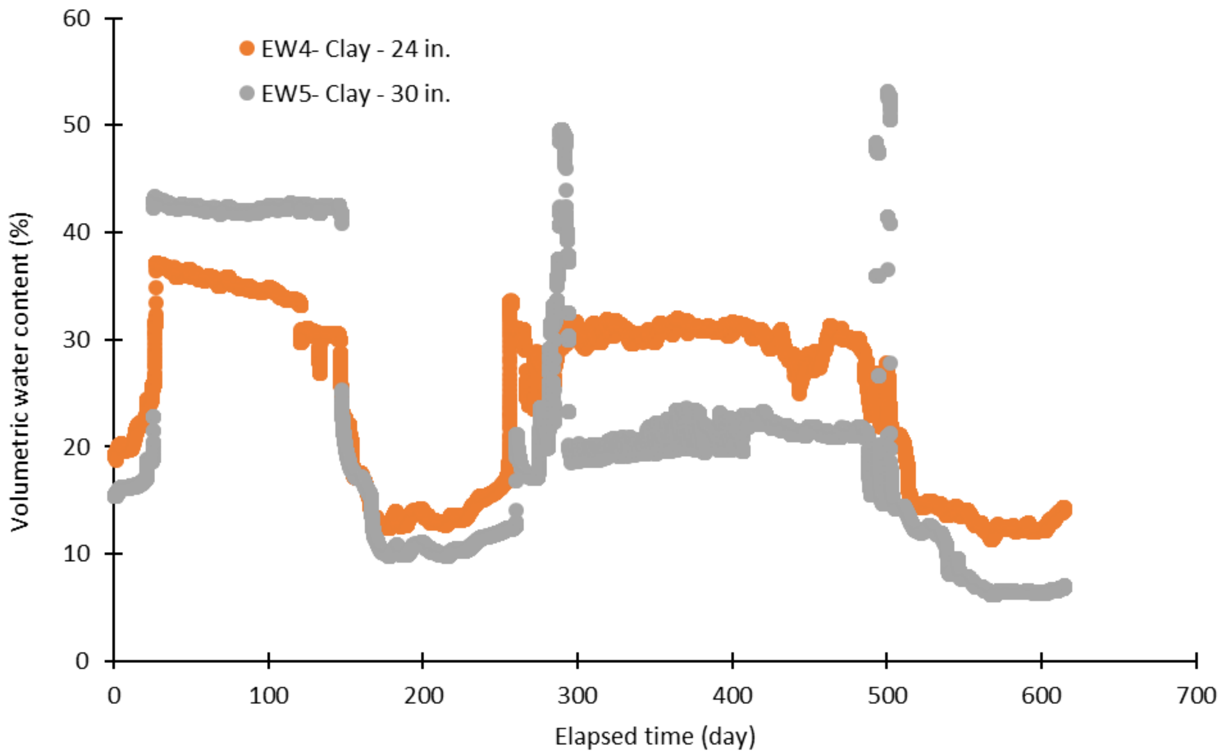

Figure 21- Variations in volumetric water content (%) in depth of clay subgrade underneath the concrete slab in Cell 138

Distress Survey

During the distress survey conducted in November 2018, a diagonal crack was observed in the traffic lane of Cell 138. The crack starts about 1.0 ft. from the intersection of the transverse and longitudinal joints and continues with an almost 45 degrees angle towards the shoulder of the inside lane as presented in Figure 22. Potential problems with base and/or subgrade may have contributed to formation of the cracks. Stresses caused by traffic loading can be another reason for cracking in this panel. The research team will monitor the crack and further investigate the potential cause for distress.

Figure 22- Cracking occurred on inside lane at Cell 138

It was reported by MnDOT staff that a transverse crack was observed on February 27, 2018, on the first panel transition from Cell 138 to 238 across both inside and outside lanes. The crack is about 5 feet from the downstream joint and angling slightly away from mid-panel as shown in Figure 23. Further cracking (Figure 24 and Figure 25) was also observed in July 2018 near the wheel path at Cell 238.

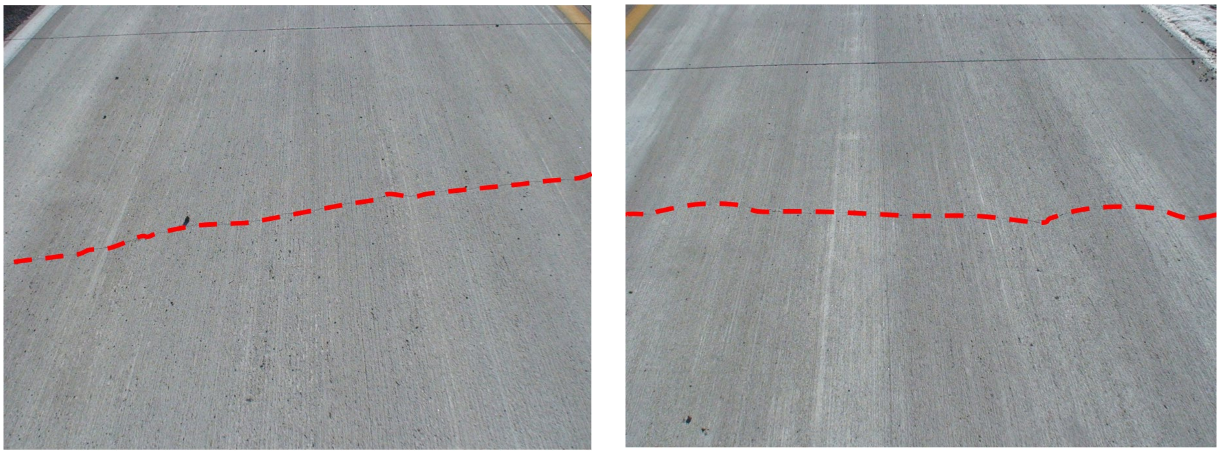

Figure 23- Transverse crack occurred on outside lane (left) and inside lane (right) at Cell 238

Site visit and coring was conducted on November 6, 2018 to further elucidate the reason for progressive cracking at Cell 238. In-situ investigations suggested that the main transverse cracking at this location was induced by the utility line underneath the pavement (Figure 25).

In collaboration with staff at MnROAD, the research team obtained four cores from Cell 238 to further investigate the reason for the observed distress. Two of these cores (C-1 and T-1) were extracted from the concrete adjacent to the transverse crack as shown in Figure 25. Core C-1 was obtained from the outside lane and core T-1 was obtained from the inside lane (exposed to traffic). Moreover, two cores were extracted (C-2 and T-2) from a panel with no cracking to serve as the reference (Figure 26). It should be noted that in each location, cores were obtained from both the inside and outside lanes to understand the potential effect of traffic loading (if any) on the observed distress. The pavement thickness at the distress area was about 8.0 in. compared to 9.0 in. for the panel with no sign of distress.

Figure 24- Further distress in form of cracking near the wheel path at Cell 238

Figure 25- Distress in form of cracking near the wheel path at Cell 238

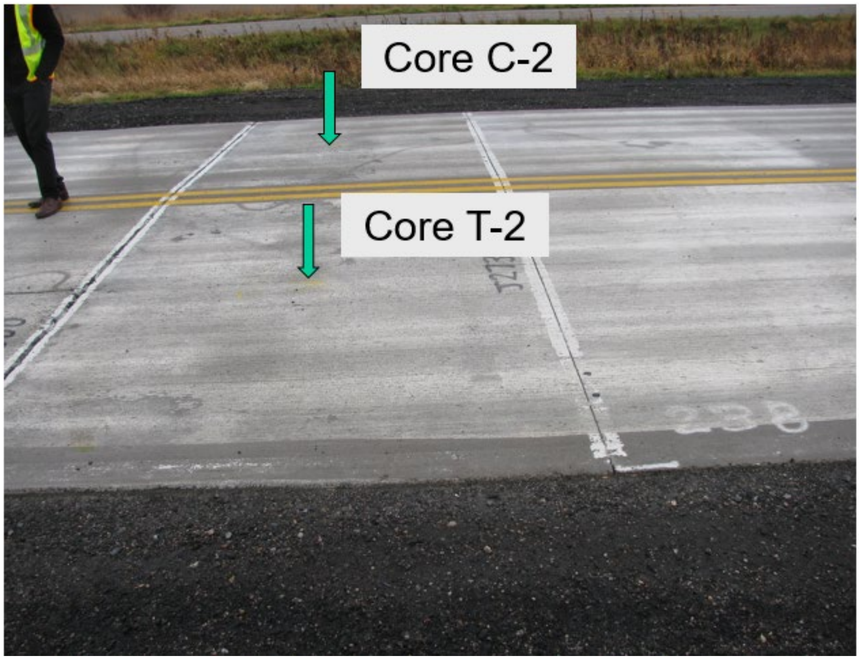

Figure 26- Panel with no cracking at the beginning of Cell 238 to serve as reference

Borehole permeability test was also conducted to compare the permeability of the base layer at the coring spots (ASTM D6391). This test involves monitoring the rate of water infiltration trough the base layer using a standpipe with a falling head. The test setup is presented in Figure 27.

Figure 27- Borehole permeability test setup

Drop in water level was monitored over time and the average rate of flow during periods of stable measurements was reported for each coring spot. Stable readings were obtained for core holes number T-1, T-2, and C-2. However, the run off through concrete cracks made it impossible to obtain stable readings for the C-1 location. Higher base permeability was observed for the area with no distress as presented in Table 15.

Table 15- Data obtained from testing core samples and core holes

Core ID	Pavement Thickness (in.)	Location	Surface Resistivity (kohm-cm)	Base Permeability (ft/day)
T-1	7.75	Distressed area, Cell 238	95.0	1.78
C-1	8.0		90.5	N/A
T-2	8.875	Area with no distress, Cell 238	81.0	5.20
C-2	9.0		90.0	4.93

The visual inspection of the Core T-1, extracted from the main distressed area revealed segregation of coarse aggregates from mortar as presented in Figure 28. No such problem was observed for the rest of the cores. Such a segregation can lead to limited contribution of coarse aggregates in restraining the mortar during shrinkage. Moreover, reduced local modulus of elasticity, along with the stresses exerted by traffic loading in the area adjacent to the transverse crack can be considered as the other contributors to the distress observed in Cell 238. Potential problems with base and/or subgrade can also contribute to formation of the cracks as a result of punching forces exerted by the traffic load.

Cores were transported back to the laboratory at Iowa State University for further investigation, including electrical resistivity measurement. The samples were cured in water for 7 days to ensure comparable moisture conditions. Resistivity data are summarized in Table 15. Comparable resistivity data was observed for all four cores.

Figure 28- Segregation of coarse aggregate in distress area; Core T-1 (Left) and corresponding core hole (Right)

As of November 2018, the distress in Cells 138 and 23 was limited to the reported cracks. So far the in-situ inspection of the cells exposed to environmental conditions and traffic loading, indicated proper quality of the pavement surfaces at both cells. No issues were observed for the surface texture at Cell 138. Finishing problems were occasionally observed at pavement surfaces in Cell 238. This is believed to be due to the lower workability of the mixtures with lower cementitious materials content as stated in previous reports. Figure 29 presents examples of typical surface quality at Cell 138, along with the observed finishing problems at Cell 238.

Figure 29- Typical surface quality at Cell 138 (top), and finishing issues observed at Cell 238 (Bot.)

KEY FINDINGS

Based on the presented results, the following findings are developed:

- The pavement cast with low and lower cementitious materials exhibited comparable LTE with average values ranging from 80% to 97%, while lower LTE was observed for the reference concrete with average values of 88±3%. The LTE was slightly higher for the departure traffic, i.e. test after joint.
- Both pavements cast with low or lower cementitious content had similar response to the controlled traffic loading, in terms of the general deformation pattern and the recorded maximum and minimum values.
- The long-term in-situ deformations were limited to 300 $\mu\varepsilon$ for both mixtures, where variation in direction of stresses and strains seem to be dominated by shrinkage and/or moisture gradient in concrete depth.
- Temperature gradient of over 2°C/in. (3.6°F/in.) was observed in concrete pavement of Cell 138.
- Higher VWC values were observed for the clay layer compared to the Class 5 aggregate base. VWC data seems to be highly affected by the temperature variations, where severe drop in VWC (%) was observed with sub-zero temperatures.
- In-situ inspection indicated proper performance of the investigated cells during the first two years. Distress observed at Cell 238 was attributed to the segregation of concrete that caused further cracking adjacent to the existing transverse crack induced by utility line.
- Finishing problems were observed in some areas of Cell 238 which is in agreement with data obtained from workability measurements during the paving. The mixture prepared with low cementitious materials content of 500 lb/yd^{3}exhibited acceptable workability based on VKelly and Box test results. Slight workability problems were observed for the mixture with lower cementitious materials content of 470 lb/yd^3.
- Overall pavements cast with optimized concrete mixtures with reduced cementitious materials content exhibited satisfactory performance over the first two years. Data will be collected during the third year and results will be further analyzed in following annual performance reports.

REFERENCES

American Association of State Highway and Transportation Officials (AASHTO). 2011. Standard Method of Test for Surface Resistivity Indication of Concrete's Ability to Resist Chloride Ion Penetration. AASHTO TP 95. AASHTO, Washington, DC.

American Association of State Highway and Transportation Officials (AASHTO). 2017. Standard Method of Vibrating Kelly Ball (VKelly) Penetration in Fresh Portland Cement Concrete. AASHTO TP 129. AASHTO, Washington, DC.

ASTM D6391-11, Standard Test Method for Field Measurement of Hydraulic Conductivity Using Borehole Infiltration, ASTM International, West Conshohocken, PA, 2011

ASTM E2583-07(2015), Standard Test Method for Measuring Deflections with a Light Weight Deflectometer (LWD), ASTM International, West Conshohocken, PA, 2015

ASTM E950 / E950M-09(2018), Standard Test Method for Measuring the Longitudinal Profile of Traveled Surfaces with an Accelerometer-Established Inertial Profiling Reference, ASTM International, West Conshohocken, PA, 2018

http://www.dot.state.mn.us/mnroad/data/pdfs/semidescription.pdf

Minnesota Department of Transportation (MnDOT). 2013. MnROAD Semi Tractor Trailrer. MnDOT, St. Paul, MN.

Minnesota Department of Transportation (MnDOT). 2013. Moisture Sensing Documentation. MnDOT, St. Paul, MN. http://www.dot.state.mn.us/mnroad/pdfs/Moisture%20Sensing%20at%20MnROAD(working%20document).pdf

Minnesota Department of Transportation (MnDOT). 2016. Standard Specifications for Construction. Section 2301: Concrete Pavement. MnDOT, St. Paul, MN. https://www.dot.state.mn.us/materials/concretedocs/Section_3_2301_Specifications.pdf

APPENDIX

Temperature data obtained at Station 9390.8:

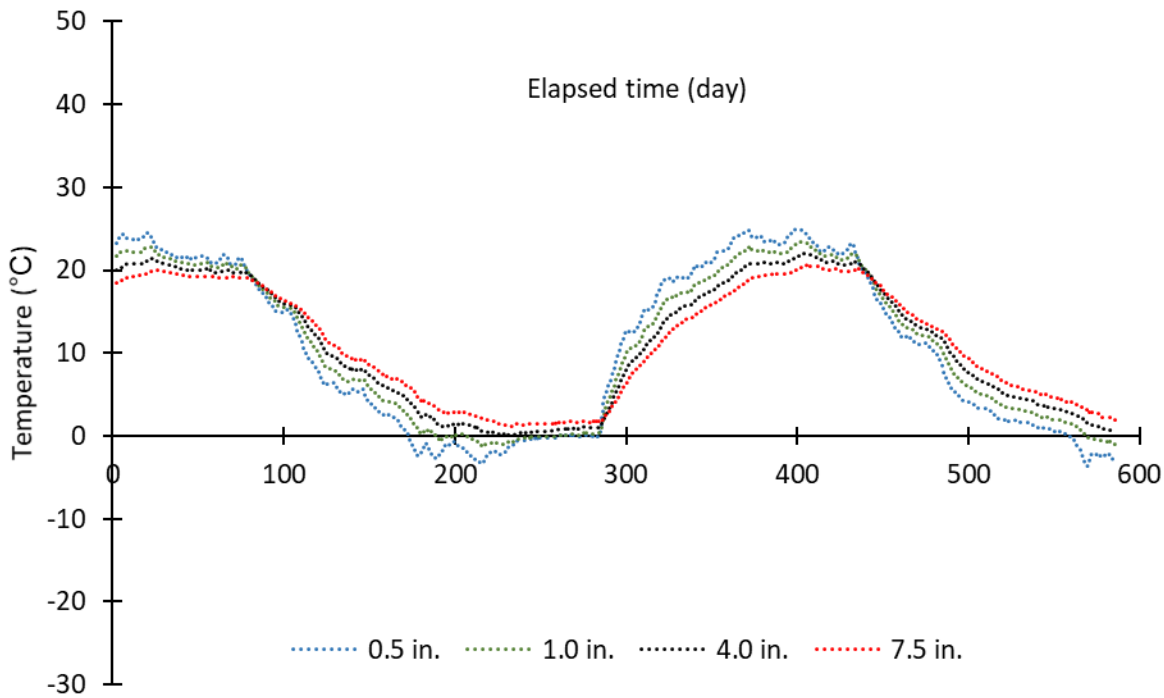

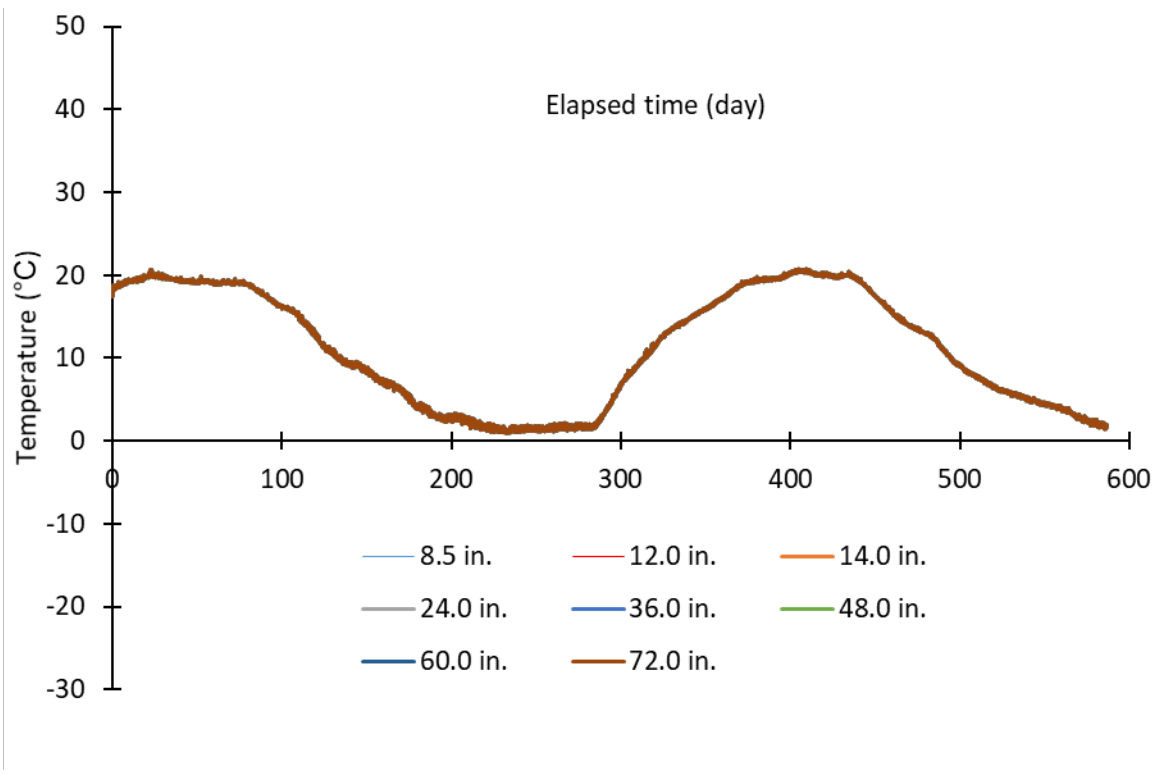

EW data obtained for sensors EC001 and EC002 embedded in concrete: